Proceedings of
ASME TURBO EXPO 2001
June 4-7, 2001, New Orleans, Louisiana

2001-GT-0196

ASME 2001 Gas Turbine Conference

Improved Prediction of Turbomachinery Flows using Near-Wall Reynolds-Stress Model

G.A. Gerolymos, J. Neubauer, V.C. Sharma, and I. Vallet

Université Pierre-et-Marie-Curie, 91405 Orsay, Paris, France

Abstract

In this paper an assessment of the improvement in the prediction of complex turbomachinery flows using a new near-wall Reynolds-stress model is attempted. The turbulence closure used is a near-wall low-turbulence-Reynolds-number Reynolds-stress model, that is independent of the distance-from-the-wall and of the normal-to-the-wall direction. The model takes into account the Coriolis redistribution effect on the Reynolds-stresses. The 5 mean flow equations and the 7 turbulence model equations are solved using an implicit coupled $O(\Delta x^3)$ upwind-biased solver. Results are compared with experimental data for 3 turbomachinery configurations: the NTUA *high subsonic annular cascade, the* NASA_37 *rotor, and the* RWTH $1\frac{1}{2}$*stage turbine. A detailed analysis of the flowfield is given. It is seen that the new model that takes into account the Reynolds-stress anisotropy substantially improves the agreement with experimental data, particularily for flows with large separation, while being only 30% more expensive than the* $k-\varepsilon$ *model (thanks to an efficient implicit implementation). It is believed that further work on advanced turbulence models will substantially enhance the predictive capability of complex turbulent flows in turbomachinery.*

Introduction

Computational Fluid Dynamics (CFD) coupled to turbomachinery specific steady [1] [2] [3] and unsteady [4] [5] [6] models, and supported by carefully planed experiments [7] [8] [9], has greatly enhanced our understanding of the complex flow phenomena encountered in mulststage turbomachinery [10] [11]. There are 3 major research areas where progress is necessary for improving the predictive capability of computational methodologies:

1) Correct modelling of steady and unsteady multistage effects [11] [12]
2) Inclusion of technological details [13] [14] [15], which is mainly a multiblock structured or unstructured grid management issue
3) Turbulence and transition modelling [16] [17] [18]

An examination of computational methodologies for steady and unsteady turbomachinery flows (Table 1) indicates that the Boussinesq hypothesis of tensorial proportionality between the Reynolds-stresses and the mean flow rate-of-deformation tensor [16] is almost invariably used, the more advanced models solving 2 transport equations (an equation for the turbulence kinetic energy and an appropriate scale-determining equation). Although 2-equation models give better results than mixing-length models (and are independent of grid topology) they do not take into account the anisotropy of the Reynolds-stress tensor. More importantly they ignore the misalignement of the Reynolds-stress tensor and the mean flow rate-of-deformation tensor, which can be important in complex 3-D separated flows. Numerous variants of 2-equation models exist, but globally results are very similar between variants. In order to improve upon the 2-equation family, it seems necessary to use models that handle properly the Reynolds-stress tensor anisotropy. To the authors knowledge such models have not yet been evaluated for 3-D turbomachinery applications.

The Reynolds-stress models (RSM) are 7-equation closures, solving 6 transport equations for the 6 components of the symmetric Reynolds-stress tensor, and 1 scale-determining equation [65] [66] [67]. An additional interest of these models for turbomachiney applications is that the transport equations for the Reynolds-stresses contain exact Coriolis redistribution terms, and as a consequence take naturally into account the effect of rotation on turbulence. Recently a Reynolds-stress closure for compressible sepa-

Table 1: Turbulence models used in 3-D turbomachinery CFD

authors	date	closure	model	space	time
Hah [19]	1986	2-eq	ARSM [20]	$O(\Delta x^2)$ upwind	implicit PB
Dawes [21] [2] [22]	1987	0-eq	ML [23]	$O(\Delta x^2)$ centered	implicit
Hah [24] [25] [26]	1988	2-eq	$\mathrm{k}-\varepsilon$ [27]	$O(\Delta x^2)$ upwind	implicit PB
Adamczyk et al. [28] [29] [30]	1990	0-eq	ML [23]	$O(\Delta x^2)$ centered	RK + IRS
Chima [31] [32]	1990	0-eq	ML [23]	$O(\Delta x^2)$ centered	RK + IRS
Lakshminarayana et al. [33] [34] [35]	1992	2-eq	$\mathrm{k}-\varepsilon$ [27]	$O(\Delta x^2)$ centered	RK
Denton [3]	1992	0-eq	ML [3]	$O(\Delta x^2)$ centered	explicit + MLTGRD
Dawes [36] [37]	1992	2-eq	$\mathrm{k}-\varepsilon$ [38]	$O(\Delta x^2)$ centered†	RK + IRS
Hirsch et al. [39] [40]	1993	0-eq	ML [23]	$O(\Delta x^2)$ centered	RK + IRS
Arnone [41] [43] [42]	1993	0-eq	ML [23]	$O(\Delta x^2)$ centered	RK + IRS + MLTGRD
Turner and Jennions [44] [45]	1993	2-eq	$\mathrm{k}-\varepsilon$ WF [46]	$O(\Delta x^2)$ centered	RK
Vogel et al. [47] [48]	1997	2-eq	$\mathrm{k}-\omega_{\mathrm{T}}$ [49]	$O(\Delta x^2)$ centered	RK
Ameri et al. [50] [51]	1998	2-eq	$\mathrm{k}-\omega_{\mathrm{T}}$ [49]	$O(\Delta x^2)$ centered	RK + IRS + MLTGRD
Furukawa et al. [52]	1998	0-eq	ML [23]	$O(\Delta x^3)$ upwind	implicit
Rhie et al. [53] [54]	1998	2-eq	$\mathrm{k}-\varepsilon$ WF [46]	$O(\Delta x^2)$ centered	implicit PB
Gerolymos and Vallet [55] [56] [57]	1998	2-eq	$\mathrm{k}-\varepsilon$[58]	$O(\Delta x^3)$ upwind	implicit
Arima et al. [59]	1999	2-eq	$\mathrm{k}-\varepsilon$[27]	$O(\Delta x^3)$ TVD	implicit
Fritsch et al. [60] [61]	1999	2-eq	$\mathrm{k}-\varepsilon$ WF [46]	$O(\Delta x^2)$ centered	RK + IRS
Sayma et al. [63]	2000	1-eq	1-eq [64]	$O(\Delta x^2)$ centered†	implicit
present	2000	7-eq	RSM [68] [69]	$O(\Delta x^3)$ upwind	implicit

WF = wall-functions ; IRS = implicit residual smoothing ; PB = pressure-based ; RK = Runge-Kutta ; MLTGRD = multigrid ; ML = mixing-length ; ARSM = algebraic Reynolds-stress model ; RSM = Reynolds-stress model ; † unstructured

rated flows, that is independent of the distance-from-the-wall and of the normal-to-the-wall direction, and that includes near-wall terms allowing integration to the wall, has been developed [68] and validated for a number of configurations [70] [71]. This closure has also been extended to rotating flows [69].

The purpose of the present work is to examine the predictive capability of this RSM closure for turbomachinery configurations, and to assess potential improvements compared to 2-equation closures. Results are presented for 3 turbomachinery configurations:

1) The NTUA subsonic ($\check{M} < 0.7$) annular cascade [72] [73] [74], a stator with thin rotor-like profiles, subjected to inflow with important radial gradients and exhibiting a large separation at the hub, that computations using the Launder-Sharma $\mathrm{k}-\varepsilon$ closure fail to predict.

2) The NASA_37 rotor, a well-known turbomachinery testcase [75] [76] [77] [78], for which mixing-length and 2-equation closures fail to correctly predict the nominal-speed operating line.

3) The RWTH $1\frac{1}{2}$stage turbine [79] [80], for which results using the Launder-Sharma $\mathrm{k}-\varepsilon$ closure show very good agreement with measurements.

Turbulence Model

The mean flow equations and the turbulence closure used in the present work are described in detail by Gerolymos and Vallet [68] [69], and are summarized in the following for completeness. The transport equations for the mean-flow (Eqs 1–3), and the Reynolds-stresses (Eq. 4), are written in a Cartesian reference-frame rotating with constant (time-independent) rotational velocity $\vec{\Omega} = \Omega_i \vec{e}_i$

$$\frac{\partial\bar{\rho}}{\partial t} + \frac{\partial\bar{\rho}\tilde{W}_\ell}{\partial x_\ell} = 0 \quad (1)$$

$$\frac{\partial\bar{\rho}\tilde{W}_i}{\partial t} + \frac{\partial}{\partial x_\ell}[\bar{\rho}\tilde{W}_i\tilde{W}_\ell + \bar{p}\delta_{i\ell}] + 2\bar{\rho}\epsilon_{ij\ell}\Omega_j\tilde{W}_\ell + \bar{\rho}\frac{\partial}{\partial x_i}[-\tfrac{1}{2}\Omega^2R^2] - \frac{\partial}{\partial x_\ell}[\bar{\tau}_{i\ell} - \bar{\rho}\widetilde{w_i''w_\ell''}] = 0 \quad (2)$$

$$\frac{\partial}{\partial t}[\bar{\rho}(\check{h}_{t\mathrm{W}} - \tfrac{1}{2}\Omega^2R^2) - \bar{p}] + \frac{\partial}{\partial x_\ell}[\bar{\rho}\tilde{W}_\ell(\check{h}_{t\mathrm{W}} - \tfrac{1}{2}\Omega^2R^2)] - \frac{\partial}{\partial x_\ell}[\tilde{W}_i(\bar{\tau}_{i\ell} - \bar{\rho}\widetilde{w_i''w_\ell''}) - (\bar{q}_\ell + \bar{\rho}\widetilde{h''w_\ell''})] = \underbrace{-(P_\mathrm{k} - \bar{\rho}\varepsilon + \overline{p'\frac{\partial w_\ell''}{\partial x_\ell}}) + \frac{\partial}{\partial x_\ell}[\overline{pw_\ell''}] + (-\bar{p}\delta_{i\ell} + \bar{\tau}_{i\ell})\frac{\partial\overline{w_i''}}{\partial x_\ell}}_{S_{\check{h}_t}} \quad (3)$$

$$\underbrace{\frac{\partial\bar\rho\widetilde{w_i''w_j''}}{\partial t}+\frac{\partial}{\partial x_\ell}(\bar\rho\widetilde{w_i''w_j''}\tilde W_\ell)}_{\text{convection } C_{ij}}=\underbrace{\frac{\partial}{\partial x_\ell}(-\bar\rho\widetilde{w_i''w_j''w_\ell''}-\overline{p'w_j''}\delta_{i\ell}-\overline{p'w_i''}\delta_{j\ell}+\overline{w_i''\tau_{j\ell}'+w_j''\tau_{i\ell}'})}_{\text{diffusion } d_{ij}}$$

$$+\underbrace{\overline{p'\left(\frac{\partial w_i''}{\partial x_j}+\frac{\partial w_j''}{\partial x_i}-\tfrac{2}{3}\frac{\partial w_k''}{\partial x_k}\delta_{ij}\right)}}_{\text{redistribution } \phi_{ij}}+\underbrace{\left(-2\bar\rho\epsilon_{i\ell m}\Omega_\ell\widetilde{w_j''w_m''}-2\bar\rho\epsilon_{j\ell m}\Omega_\ell\widetilde{w_i''w_m''}\right)}_{\text{Coriolis redistribution } G_{ij}}+\underbrace{\left(-\bar\rho\widetilde{w_i''w_\ell''}\frac{\partial\tilde W_j}{\partial x_\ell}-\bar\rho\widetilde{w_j''w_\ell''}\frac{\partial\tilde W_i}{\partial x_\ell}\right)}_{\text{production } P_{ij}}$$

$$-\underbrace{\left(\overline{\tau_{j\ell}'\frac{\partial w_i''}{\partial x_\ell}+\tau_{i\ell}'\frac{\partial w_j''}{\partial x_\ell}}\right)}_{\text{dissipation } \bar\rho\varepsilon_{ij}}+\underbrace{\tfrac{2}{3}\overline{p'\frac{\partial w_k''}{\partial x_k}}\delta_{ij}}_{\text{pressure-dilatation}}+\underbrace{\left(-\overline{w_i''}\frac{\partial\bar p}{\partial x_j}-\overline{w_j''}\frac{\partial\bar p}{\partial x_i}+\overline{w_i''}\frac{\partial\bar\tau_{j\ell}}{\partial x_\ell}+\overline{w_j''}\frac{\partial\bar\tau_{i\ell}}{\partial x_\ell}\right)}_{\text{density fluctuation effects } K_{ij}}\quad(4)$$

where t is the time, x_ℓ the cartesian space coordinates in the relative frame-of-reference, ϵ_{ijk} the 3-order antisymmetric tensor [81], δ_{ij} the Kronecker symbol [81], R the radius (distance from the axis of rotation: $R^2=[x_i-|\Omega|^{-2}x_j\Omega_j\Omega_i][x_i-|\Omega|^{-2}x_j\Omega_j\Omega_i]$), W_i the relative velocity components, $V_i=W_i+\epsilon_{ijk}\Omega_j x_k$ the absolute velocity components, ρ the density, p the pressure, τ_{ij} the viscous stresses, $(\tilde\cdot)$ Favre-averaging, $(\bar\cdot)$ nonweighted-averaging, $(\cdot'')$ Favre-fluctuations, $(\cdot')$ nonweighted-fluctuations, $\breve h_{t_{\rm W}}=\tilde h+\frac{1}{2}\tilde W_i\tilde W_i$ the total enthalpy of the relative mean flow (which is different from the Favre-averaged total enthalpy $\tilde h_{t_{\rm W}}=\tilde h+\frac{1}{2}\tilde W_i\tilde W_i+{\rm k}=\breve h_{t_{\rm W}}+{\rm k}$), h the specific enthalpy, ${\rm k}=\frac{1}{2}\widetilde{w_i''w_i''}$ the turbulence-kinetic-energy, w_i'' the frame-independent velocity fluctuations, $P_{\rm k}=\frac{1}{2}P_{\ell\ell}$ the turbulence kinetic energy production (equal to the trace of the Reynolds-stresses production tensor P_{ij}), and ε the dissipation-rate of the turbulence kinetic energy (equal to the trace of the Reynolds-stresses dissipation-rate tensor ε_{ij}. The symbol $(\breve\cdot)$ is used to denote a function of average quantities that is neither a Favre-average nor a nonweighted average. The above equations are exact Favre-Reynolds-averaged unclosed equations.

Convection C_{ij}, Coriolis redistribution G_{ij}, and production P_{ij} are exact terms. In the present model [68] [69] direct compressibility effects K_{ij}, pressure-dilatation correlation, and pressure-diffusion are neglected. The triple correlations are modelled following Hanjalić and Launder [82]. The major improvements in the present model concern the pressure-strain redistribution terms. The pressure-strain redistribution terms augmented by the dissipation tensor anisotropy [83] are split into the slow and rapid parts and the corresponding echo-terms. The slow part ϕ_{ij1} is modelled by a simple quasi-linear return-to-isotropy model whose coefficient has been optimized by Launder and Shima [83] so as to account also for the anisotropic part of the dissipation tensor $\varepsilon_{ij}-\frac{2}{3}\delta_{ij}\varepsilon$. The closure for the rapid terms uses an isotropization-of-absolute-flow-production model [84] [85] [86]. The echo terms are computed in the usual way [87] but the unit pseudonormal direction $\vec e_n=n_i\vec e_i$ is approximated by the gradient of a function of the turbulence lengthscale $\ell_{\rm T}$, of the anisotropy tensor invariants, and of the Lumley flatness parameter A [88] thus making the model independent of wall topology [89]. The effect of the distance-from-the-wall is included in the functions C_1^w and C_2^w. The final model is

$$K_{ij}\cong 0\quad;\quad\overline{p'\frac{\partial w_\ell''}{\partial x_\ell}}\cong 0\quad;\quad\overline{pw_\ell''}\cong 0$$

$$\overline{w_i''}\cong 0\quad;\quad S_{\breve h_t}\cong-(P_{\rm k}-\rho\varepsilon)\quad(5)$$

$$d_{ij}\cong\frac{\partial}{\partial x_k}[-\bar\rho\widetilde{w_i''w_j''w_k''}+\breve\mu\frac{\partial\widetilde{w_i''w_j''}}{\partial x_k}]\quad(6)$$

$$\widetilde{w_i''w_j''w_k''}\cong-C_s\frac{\rm k}{\varepsilon}\left[\widetilde{w_i''w_\ell''}\frac{\partial\widetilde{w_j''w_k''}}{\partial x_\ell}+\widetilde{w_j''w_\ell''}\frac{\partial\widetilde{w_k''w_i''}}{\partial x_\ell}+\widetilde{w_k''w_\ell''}\frac{\partial\widetilde{w_i''w_j''}}{\partial x_\ell}\right]\quad;\quad C_s=0.11\quad(7)$$

$$\begin{aligned}\phi_{ij}-\bar\rho\varepsilon_{ij}&=\left[\phi_{ij}-\bar\rho(\varepsilon_{ij}-\tfrac{2}{3}\delta_{ij}\varepsilon)\right]\\&=\phi_{ij1}+\phi_{ij2}+\phi_{ij1}^w+\phi_{ij2}^w-\tfrac{2}{3}\delta_{ij}\varepsilon\\&\cong-C_1\bar\rho\varepsilon a_{ij}-C_2\left(P_{ij}+\tfrac{1}{2}G_{ij}-\tfrac{1}{3}\delta_{ij}P_{\ell\ell}\right)\end{aligned}$$

$$+C_1^w\frac{\varepsilon}{k}\left[\bar\rho\widetilde{w_k''w_m''}n_kn_m\delta_{ij}-\tfrac{3}{2}\bar\rho\widetilde{w_k''w_i''}n_kn_j-\tfrac{3}{2}\bar\rho\widetilde{w_k''w_j''}n_kn_i\right]$$

$$+C_2^w\left[\phi_{km2}n_kn_m\delta_{ij}-\tfrac{3}{2}\phi_{ik2}n_kn_j-\tfrac{3}{2}\phi_{jk2}n_kn_i\right]-\tfrac{2}{3}\delta_{ij}\varepsilon\quad(8)$$

The model coefficients (C_1, C_2, C_1^w, C_2^w) are functions of the anisotropy tensor (A_2, A_3, A) and of the turbulence-Reynolds-number $Re_{\rm T}$ (Table 2). The pseudonormal direction $\vec n$ appearing in the echo terms is given by the direction of the gradient of a function of turbulence length-scale $\ell_{\rm T}$ and of the anisotropy tensor invariants (Table 2).

The dissipation-rate of the turbulence-kinetic-energy ε is estimated by solving a transport equation for the modified-dissipation-rate [93] $\varepsilon^*=\varepsilon-2\breve\nu({\rm grad}\sqrt{\rm k})^2$ ($\breve\nu$ the kinematic viscosity). The wall boundary-condition is $\varepsilon_w^*=0$, offering enhanced numerical stability.

Table 2: Anisotropy tensor invariants and model functions for the pressure-strain closure (Eq. 8)

$$a_{ij} = \frac{\widetilde{w_i''w_j''}}{\mathrm{k}} - \tfrac{2}{3}\delta_{ij} \quad ; \quad A_1 = a_{ii} = 0 \quad ; \quad A_2 = a_{ik}a_{ki} \quad ; \quad A_3 = a_{ik}a_{kj}a_{ji} \quad ; \quad A = \left[1 - \tfrac{9}{8}(A_2 - A_3)\right]$$

$$C_1 = 1 + 2.58 A A_2^{\frac{1}{4}} \left[1 - \mathrm{e}^{-(\frac{Re_\mathrm{T}}{150})^2}\right]$$

$$C_2 = \min[1, 0.75 + 1.3\max[0, A - 0.55]] A^{[\max(0.25, 0.5 - 1.3\max[0, A-0.55])]} [1 - \max(0, 1 - \tfrac{Re_\mathrm{T}}{50})]$$

$$\vec{e}_n = n_i\vec{e}_i = \frac{\mathrm{grad}\ell_n}{||\mathrm{grad}\ell_n||} \quad ; \quad \ell_n = \frac{\ell_\mathrm{T}[1 - \mathrm{e}^{-\frac{Re_\mathrm{T}}{30}}]}{1 + 2\sqrt{A_2} + A^{16}} \quad ; \quad \ell_\mathrm{T} = \frac{\mathrm{k}^{\frac{3}{2}}}{\varepsilon}$$

$$C_1^w = 0.83\,[1 - \tfrac{2}{3}(C_1 - 1)]\ \ ||\mathrm{grad}\ell_1^w|| \quad ; \quad \ell_1^w = \frac{\ell_\mathrm{T}[1 - \mathrm{e}^{-\frac{Re_\mathrm{T}}{30}}]}{1 + 2A_2^{0.8}}$$

$$C_2^w = \max\left[\frac{2}{3} - \frac{1}{6C_2}, 0\right]\ \ ||\mathrm{grad}\ell_2^w|| \quad ; \quad \ell_2^w = \frac{\ell_\mathrm{T}[1 - \mathrm{e}^{-\frac{Re_\mathrm{T}}{30}}]}{1 + 1.8A_2^{\max(0.6, A)}}$$

The modelled Launder-Sharma [58] equation, with a tensorial diffusion coefficient [90] is used

$$\frac{\partial \bar\rho\varepsilon^*}{\partial t} + \frac{\partial}{\partial x_\ell}\left(\tilde{W}_\ell\bar\rho\varepsilon^*\right) - \frac{\partial}{\partial x_\ell}\left[\left(\breve\mu\delta_{k\ell} + C_\varepsilon\frac{\mathrm{k}}{\varepsilon^*}\bar\rho\widetilde{w_k''w_\ell''}\right)\frac{\partial\varepsilon^*}{\partial x_k}\right] =$$

$$C_{\varepsilon 1}P_\mathrm{k}\frac{\varepsilon^*}{\mathrm{k}} - C_{\varepsilon 2}\bar\rho\frac{\varepsilon^{*2}}{\mathrm{k}} + \frac{2\breve\mu\mu_\mathrm{T}}{\bar\rho}(\nabla^2\,\tilde{\vec{W}})^2 \quad (9)$$

$$C_\varepsilon = 0.18 \ ; \ C_{\varepsilon 1} = 1.44 \ ; \ C_{\varepsilon 2} = 1.92(1 - 0.3\mathrm{e}^{-Re_\mathrm{T}^{*2}}) \quad (10)$$

The turbulent heat-flux $\bar\rho\widetilde{h''w_i''}$ is closed by a simple gradient model [68]

$$\bar\rho\widetilde{h''w_i''} = -\frac{\mu_\mathrm{T}c_p}{Pr_\mathrm{T}}\frac{\partial\tilde T}{\partial x_i} \ ; \ c_p = \frac{\gamma}{\gamma - 1}R_g \ ; \ \mu_\mathrm{T} = C_\mu\breve\mu Re_\mathrm{T}^*$$

$$C_\mu = 0.09\mathrm{e}^{-\frac{3.4}{(1 + 0.02Re_\mathrm{T}^*)^2}} \ ; \ Re_\mathrm{T}^* = \frac{\bar\rho\mathrm{k}^2}{\breve\mu\varepsilon^*} \quad (11)$$

where c_p is the heat capacity at constant pressure, Pr_T the turbulent Prandtl number (in the present work $Pr_\mathrm{T} = 0.9$ to obtain the correct recovery temperature for turbulent flow over an adiabatic wall), and Re_T^* the turbulence Reynolds number based on the modified dissipation [93] $\varepsilon^* = \varepsilon - 2\breve\nu(\mathrm{grad}\sqrt{\mathrm{k}})^2$ (ε being turbulence-kinetic energy dissipation, and $\breve\nu$ the kinematic viscosity). The thermodynamics of the working gas and the mean viscous stresses and heat-flux are approximated by standard closure assumptions [68] [90] [91]

$$\bar p = \bar\rho R_g\tilde T = \bar\rho\frac{\gamma - 1}{\gamma}\tilde h \ ; \ \breve\mu = \mu(\tilde T) = \mu_{273}\frac{\tilde T^{\frac{3}{2}}}{273.15^{\frac{3}{2}}}\frac{T_S + 273.15}{T_S + \tilde T}$$

$$\breve\kappa = \kappa(\tilde T) = \kappa_{273}\frac{\mu(\tilde T)}{\mu_{273}}[1 + A_\kappa(\tilde T - 273.15)] \quad (12)$$

$$\bar\tau_{ij} \cong \breve\mu(\frac{\partial\tilde W_i}{\partial x_j} + \frac{\partial\tilde W_j}{\partial x_i} - \tfrac{2}{3}\frac{\partial\tilde W_\ell}{\partial x_\ell}\delta_{ij}) \quad ; \quad \bar q_i \cong -\breve\kappa\frac{\partial\tilde T}{\partial x_i} \quad (13)$$

where γ is the isentropic exponent, R_g the gas-constant, μ the dynamic viscosity, and κ the heat conductivity. For air $R_g = 287.04$ m^2 s^{-2} K^{-1}, $\gamma = 1.4$, $\mu_{273} = 17.11\times10^{-6}$ Pa s, $\kappa_{273} = 0.0242$ W m^{-1} K^{-1}, $T_S = 110.4$ K, and $A_\kappa = 0.00023$ K^{-1}.

Numerics and Inflow Conditions

The computational method used is based on the solver developed by Gerolymos and Vallet [90] [91]. Turbomachinery computations use multiblock structured grids [55] [56] [57] which are generated biharmonically [92]. The mean-flow and turbulence-transport equations are written in the (x, y, z) cartesian rotating (relative) coordinates system, and are discretized in space, on a structured multiblock grid, using a 3-order upwind-biased MUSCL scheme with Van Leer flux-vector-splitting and Van Albada limiters, and the resulting semi-discrete scheme is integrated in time using a 1-order implicit procedure [91] [55] [90]. The mean-flow and turbulence-transport equations are integrated simultaneously. Source-terms (centrifugal, Coriolis, and RSM) are treated explicitly. The local-time-step is based on a combined convective (Courant) and viscous (von Neumann) criterion. The boundary conditions which are applied both explicitly and implicitly, using a phantom-nodes-technique at grid interfaces, are described in detail by Gerolymos, Tsanga and Vallet [55].

Inflow profiles of total-pressure, total-temperature and Reynolds-stresses are obtained by fitting, near the hub and the casing, analytic boundary-layer profiles of velocity, temperature and turbulence variables, in a manner similar to Gerolymos [99]. The velocity and temperature profiles are based on a van Driest [94] transformation of the Spalding profile [95], augmented by a Coles wake function [96]. Turbulence kinetic energy and dissipation-rate are obtained by a local equilibrium hypothesis $P_{\mathrm{k}} = \bar{\rho}\varepsilon^*$ (where the eddy viscosity is obtained using the Spalding profile [95] in the inner part, and Clauser's eddy-viscosity [97] in the outer-part of the boundary-layers). The Reynolds-stresses are obtained using constant flat-plate boundary-layer structure values [98]. The basic initialization procedure is 2-D. It is applied in a frame-of-reference where the wall is fixed, and with a coordinate-system aligned to the external flow-velocity. A full description of the procedure for 3-D internal flows containing solid corners is given by Vallet [100], and has been applied to turbomachinery by Tsanga [101].

Table 3: Configurations studied

	NTUA_1	NASA_37	RWTH_1
R_{HUB} (m)	0.244	0.175–0.194	0.245
R_{CASING} (m)	0.324	0.237–0.258	0.3
χ (m)	0.1	~0.056	~0.06
Re_χ	$\sim 10^6$	$1.33–2.10\times10^6$	$0.20–0.45\times10^6$
N_{B}	19	36	36–41–36
RPM	0	17188.7	3500
$\dot{m}$ (kg s^{-1})	13.2	19.2–20.9	8.2
$\pi_{\mathrm{T\text{-}T}}$	0.988	1.95–2.15	1/1.2
p_{t_i} (Pa)	97000	101325	169500
T_{t_i} (K)	288.15	288.15	305.75
T_{u_i}	4%	3%	3%
$\delta_{i_{\mathrm{HUB}}}$ (m)	0.014	0.005	0.0025
$\Pi_{i_{\mathrm{HUB}}}$	0.8	0	0
$\delta_{i_{\mathrm{CASING}}}$ (m)	0.0025	0.005	0.005
$\Pi_{i_{\mathrm{CASING}}}$	0	0	0

R_{HUB} = flowpath radius at the hub; R_{CASING} = flowpath radius at the casing; χ = chord; Re_χ = Reynolds-number based on inflow relative velocity, blade-chord, and viscosity at inflow conditions; RPM = revolutions per minute; N_{B} =number of blades; $\dot{m}$ = massflow; $\pi_{\mathrm{T\text{-}T}}$ = total-to-total pressure-ratio; p_{t_i} = inflow total-pressure; T_{t_i} = inflow total-temperature; T_{u_i} = turbulence intensity at inflow; $\delta_{i_{\mathrm{HUB}}}$ = boundary-layer thickness at inflow on the hub; $\Pi_{i_{\mathrm{HUB}}}$ = Coles parameter at inflow on the hub; $\delta_{i_{\mathrm{CASING}}}$ = boundary-layer thickness at inflow on the casing; $\Pi_{i_{\mathrm{CASING}}}$ = Coles parameter at inflow on the casing

Comparison with Measurements

Configurations Studied

The proposed Reynolds-stress closure has been assessed through comparison with measurements and with computational results using the Launder-Sharma $\mathrm{k}-\varepsilon$ closure [58], for 3 turbomachinery configurations (Table 3). For the 3 cases a careful study of grid-convergence of computational results was undertaken (Table 4). The nondimensional distance from the wall of the first grid point nearest to it $n_w^+ = \Delta n_w u_\tau \breve{\nu}_w^{-1}$ (where u_τ is the friction velocity, Δn_w the distance from the wall, and $\breve{\nu}_w$ the kinematic viscosity at the wall) is an important parameter, which, for transonic flows with boundary-layer separation, should not exceed $\frac{3}{4}$ [90].

Annular Subsonic Cascade

The experimental set up is an annular compressor cascade studied at the Laboratory of Thermal Turbomachines of the National Technical University of Athens by Doukelis et al. [72] [73] [74]. The measurements were taken at inlet Mach numbers of ~ 0.6. Although the experiment was initially intended to investigate the effects of clearance between the blade-tip and the hub, the reference case with clearance $\delta_{\mathrm{HC}} = 0$ is a very interesting test-case, because of the experimentaly observed large hub-corner-stall.

Preliminary $\mathrm{k}-\varepsilon$ computations failed to predict the large separation region, and as a consequence gave very poor agreement with measured outflow angles. The incoming flow is quite complex, because the swirl necessary to obtain the desired inlet flow-angle was experimentaly obtained by using a scroll (and not stator vanes). As a consequence inflow profiles of total-pressure $p_{t_{\mathrm{M}}}$ and flow-angle α_{M} contain important radial variations (Fig. 1). The turbulence intensity at inflow was experimentaly estimated at the high values of 3–4%. The value $T_{u_i} = 4\%$ was applied as inflow condition in the computations (Table 3).

Comparison of computed and measured pitchwise-averaged quantities at inflow and outflow planes (Fig. 1) shows substantial differences between the present RSM and the Launder-Sharma $\mathrm{k}-\varepsilon$ [58] predictions. These computations were run using grid_D of 2.3×10^6 points (Table 4). This is a rather fine grid with $n_w^+ < \frac{3}{4}$ everywhere. At the inflow plane (situated 0.2 axial chords χ_x downstream of the computational inflow plane where the inflow profiles are applied) it is seen that both models accurately simulate the radial distributions of α_{M} and $p_{t_{\mathrm{M}}}$. They show however a difference in the turbulence profiles near the hub, due to a different development from computational inflow downstream, the RSM computations predicting a lower level of turbulence near the hub (unfortunately no detailed measurements of k_{M} were available). At the outflow the RSM computations correctly predict the experimentaly mesured high swirl near the hub. This swirl is associated with a large hub-corner-stall, on the suction-side of the blades (Fig. 2). The Mach-number plots

Table 4: Computational grid summary

	UH	O	DH	TC	OZ	points†	$n^+_{w_\mathrm{B}}$	$n^+_{w_\mathrm{FP}}$
NTUA_1								
grid_B	17×47× 69	201×49× 69	51×51× 69	-	-	914 181	< 0.7	< 0.7
grid_D	17×47×141	201×53×141	91×51×141	-	-	2 269 113	< 0.7	< 0.7
grid_E	17×47×141	201×81×141	91×51×141	-	-	3 062 661	< 0.7	< 0.7
NASA_37								
grid_B	49×41× 65	201×45× 65	81×61× 65	201×11×21	201×21×31	1 149 421	< 0.3	< 1.5
grid_C	49×41×101	201×53×101	81×61×101	201×17×31	201×21×41	1 955 587	< 0.3	< 1.0
grid_D	49×41×161	201×53×161	81×61×165	201×17×41	201×21×61	3 067 042	< 0.3	< 0.5
RWTH_1								
grid_A	31×25× 51	181×31× 51	41×31× 51	181×21×21	181×21×31	1 010 772	$< 10.$	< 5.0
grid_B	31×31× 65	201×49× 65	41×41× 65	201×21×21	201×21×31	2 265 346	< 1.0	< 1.5
grid_C	31×31× 81	201×49× 81	41×41× 81	201×31×31	201×26×46	2 957 250	< 1.0	< 1.0
grid_D	31×31×121	201×49×121	41×41×121	201×31×41	201×26×61	4 359 380	< 1.0	< 0.7

UH = upstream-H-grid (axial×tangential×radial); O = blades-O-grid (around the blade×away from blade×radial); DH = downstream-H-grid (axial×tangential×radial); TC = tip-clearance-O-grid (around the blade×away from blade×radial); OZ = O-zoom-grid (around the blade×away from blade×radial); † without O-grid points overlapped by the OZ-grid; $n^+_{w_\mathrm{B}} = n^+_w$ on the blades; $n^+_{w_\mathrm{FP}} = n^+_w$ on the flowpath

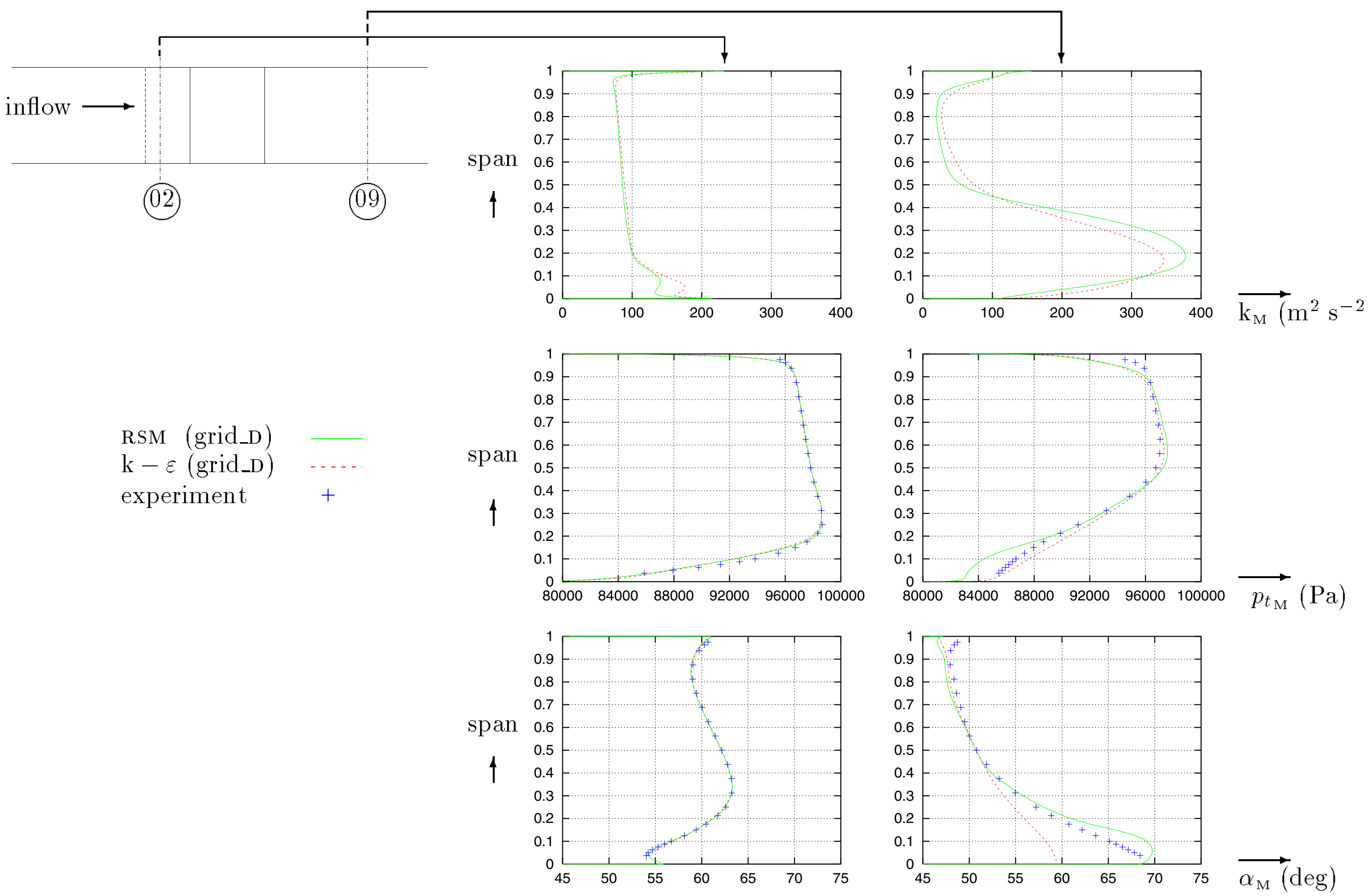

Figure 1: Comparison of measured and computed (using the present RSM and the Launder-Sharma $\mathrm{k} - \varepsilon$ [58]) pitchwise-averaged flow-angle α_M, total-pressure p_{t_M}, and turbulence-kinetic-energy $\mathrm{k_M}$ for the NTUA_1 annular cascade ($\dot{m} = 13.2$ kg s^{-1}; $T_u = 4\%$; grid_D).

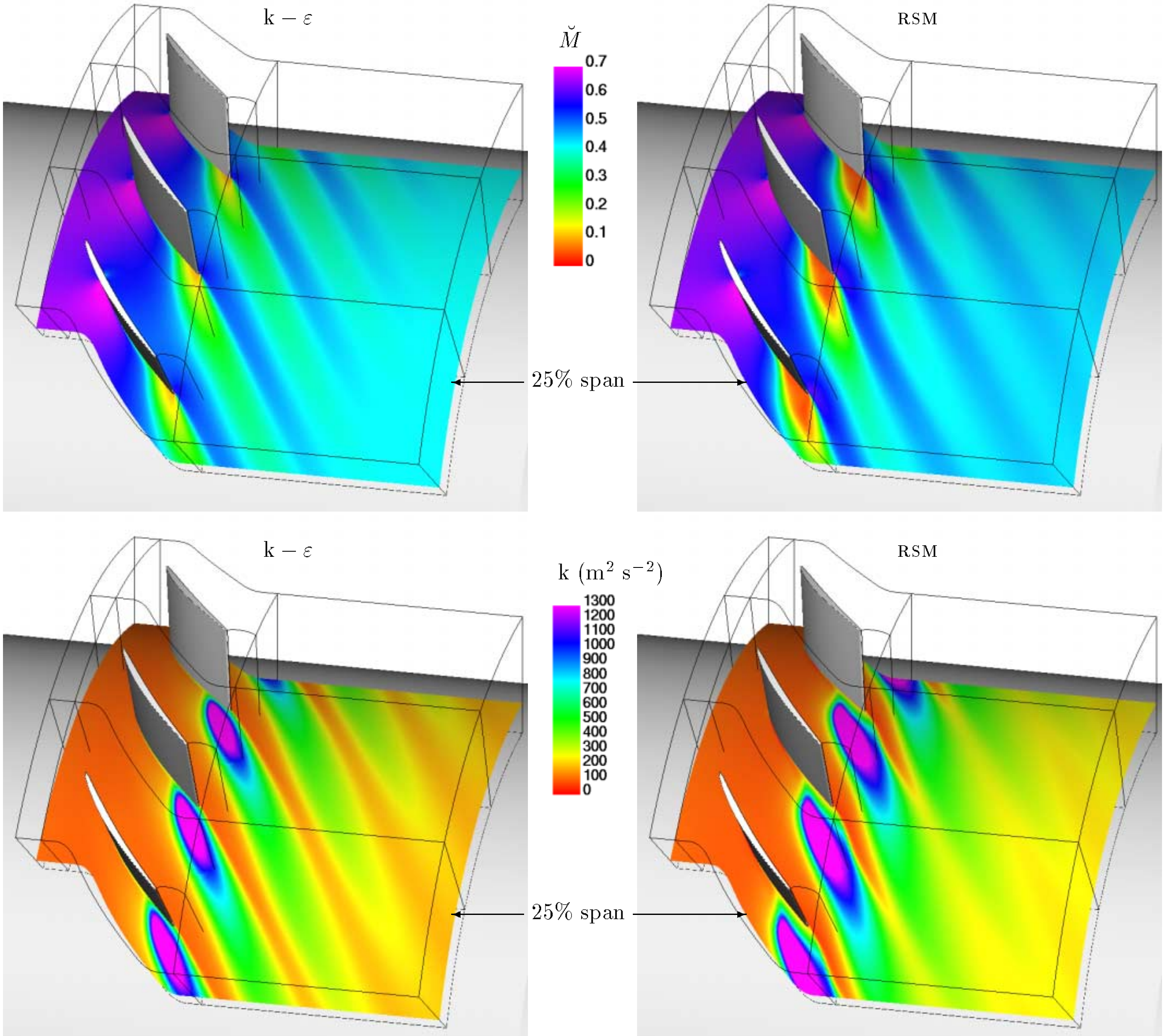

Figure 2: Comparison of Mach-number $\breve{M}$ and turbulence-kinetic-energy k computed using the present RSM and the Launder-Sharma $\mathrm{k}-\varepsilon$ [58]), at 25% span ($\dot{m} = 13.2$ kg s^{-1}; $T_u = 4\%$; grid_D).

show the large separation predicted by the RSM computations on the suction-side (Fig. 2). The flow has to go around the separation bubble, and this results to high outflow swirl at the hub (corresponding to substantial underturning at the hub), in accordance with measurements (Fig. 1). The $\mathrm{k}-\varepsilon$ computations substantially underestimate the separation region (Fig. 2), and as a consequence predict lower than measured swirl at the exit of the cascade (Fig. 1). These differences between the 2 models are also seen in the plots of turbulence-kinetic-energy k (Fig. 2), where one can also observe the larger wakes predicted by the RSM computations. Comparison of computed and measured total-pressure p_{t_M} distributions at cascade exit (Fig. 1) indicates good agreement. The RSM computations slightly overestimate losses near the hub. This, together with the slightly higher than measured values of α_M suggest that the present model slightly overestimates the separated flow region, a problem attributed rather to delayed reattachment than to extensive separation. It is indeed believed that the predicted separa-

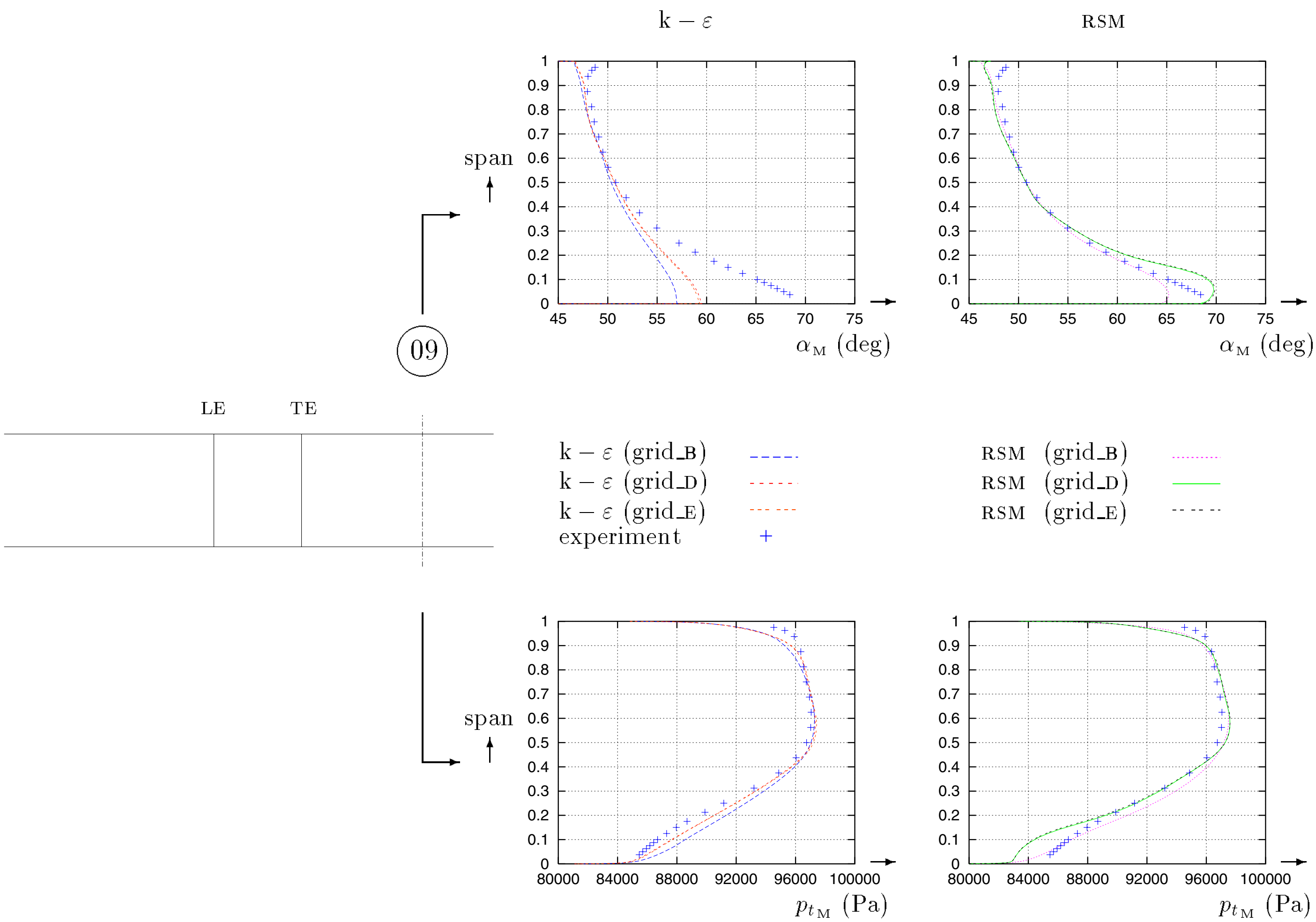

Figure 3: Study of grid-convergence of computed (using the present RSM and the Launder-Sharma $k-\varepsilon$ [58]) pitchwise-averaged flow-angle α_M, and total-pressure p_{t_M}, at the exit of the NTUA_1 annular cascade ($\dot{m} = 13.2$ kg s^{-1}; $T_u = 4\%$).

tion is not too thick, but that is does not end as abruptly as it should.

In order to assert grid independence of the results, computations were run using different grids (Table 4). Grid_B of $\sim 10^6$ points has 69 radial surfaces, and satisfactory n_w^+ (< 0.7), both on the flowpath walls and on the blades. Grid refinement strategy maintained the size of the first grid-cell away from the walls, by using more points with a lower stretching near the walls (geometric stretching was invariably used [92]). Grid_D of $\sim 2.3\times 10^6$ points has 141 radial stations, and slightly more blade-to-blade points (Table 4). Grid_E of $\sim 3\times 10^6$ points has the same radial resolution as grid_D, but a finer blade-to-blade grid (81 points from the blade surface to mid-passage, corresponding to 161 points from one blade to its neighbour), in order to examine the influence of blade-to-blade refinement (Table 4).

It should be noted that both the radial refinement (grid_B to grid_D) and the blade-to-blade refinement (grid_D to grid_E) are substantial (factor 2). Both the $k-\varepsilon$ and the RSM computations (Fig. 3) indicate that doubling the number of points radially enhances the prediction of the separation region (2.5 deg in α_M for the $k-\varepsilon$, and 4.5 deg in α_M for the RSM). The blade-to-blade refinement (grid_E) was investigated for both closures (Fig. 3), and results are identical with the results of grid_D. It is believed that grid_D is adequate, although computations with an even finer grid (radially) would be needed to demonstrate this assertion. It should be noted that even the coarse grid_B RSM computations are better than the fine grid_D $k-\varepsilon$ (Fig. 3), underlining the substantial improvement in flow angle prediction by the RSM closure. This improvement is associated with a better prediction of the separated flow structure.

Transonic Compressor Rotor

The NASA_37 transonic rotor [75] [76] [77] [78] is a well known turbomachinery test-case. Experimental data for the NASA_37 transonic rotor were obtained at various measurement planes, using both LDV (LASER Doppler Velocimetry) and classical rake measurements of p_{t_M} and T_{t_M} (the averaging procedure $(\cdot)_M$ is described in Davis et al. [76]). This rotor has 36 blades, nominal speed 17188.7 RPM, and maximum massflow at nominal speed $\dot{m}_{CH} = 20.93 \pm 0.14$ kg s^{-1}. The nominal tip-clearance-gap is 0.356 mm [75]. The measurements uncertainties were reported by Suder [78]: massflow $\dot{m}$ ± 0.3 kg s^{-1}; absolute flow angle α_M ± 1.0 deg; total pressure p_{t_M} ± 100 Pa; total temperature T_{t_M} $\pm$ 0.6 K.

Computations by numerous authors [77] [102] [13] [32] [56] [26] [59] [103], using a wide variety of turbulence models and numerical methods, highlight the predictive CFD state-of-the-art for this configuration. A carefull examination of the computations indicates that, in the limit of grid-converged results, both 0-equation and 2-equation models overestimate the total-to-total pressure ratio $\pi_{T\text{-}T}$ as a function of massflow $\dot{m}$. The 0-equation models overestimate $\pi_{T\text{-}T}$ by $\sim$ 3%, whereas the 2-equation models overestimate $\pi_{T\text{-}T}$ by $\sim$ 1.5% [103]. Grid convergence is important, as demonstrated by comparing the results using the $k-\varepsilon$ model of Chien [27] obtained by Hah and Loellbach [26] using $\sim 1.9\times10^6$ points grid and by Arima et al. [59] using $\sim 0.6\times10^6$ points. The later grid was particularly coarse in the blade-to-blade direction, and as a consequence underestimated choke massflow $\dot{m}_{CH}$ (20.77 kg s^{-1} instead of the measured value of 20.93 kg s^{-1}), which was correctly predicted by the fine grid computations by Hah and Loellbach [26]. The associated increased blockage gave a seemingly good prediction of pressure-ratio in the coarse grid computations [59], but the characteristic is translated towards lower massflow (in terms of dimensional $\dot{m}$), and the results are not representative of the grid-converged model performance.

If the form of the spanwise distribution of the pitchwise averaged total pressure p_{t_M} downstream of the rotor is considered, there are 2 regions of discrepancy with measurements: 1) a local peak of p_{t_M} near the casing, corresponding to a too strong tip-clearance vortex, and 2) a p_{t_M} deficit near the hub (this deficit is attributed to both an underestimation of hub-corner stall by the models [26] and to massflow leakage emanating from a small gap between the stationary and rotating parts of the hub upstream of the rotor [13] which was not modelled in the computations).

Previous studies by the authors [55] [56] using the same grid-generation methodology [92] and the same numerical scheme, but with the Launder-Sharma $k-\varepsilon$ turbulence model [58], include grid-convergence studies using 1, 2, and 3×10^6 points (Table 3), indicating that results with grid_C (2×10^6 points) are practically grid independent. Based on these results, all the computations presented here were run on grid_D of $\sim 3\times10^6$ points (Table 3). The computational grid consists of an H–O–H grid with 161 radial stations. Tip clearance is discretized using an independent O-type grid with 41 radial stations [55] [92]. Comparison of the measured characteristic ($\pi_{T\text{-}T}$ between stations 1 and 4 *vs.* $\dot{m}$) at nominal speed (Fig. 4) with computations using the new RSM closure [69] and the Launder-Sharma $k-\varepsilon$ turbulence model [58] indicate that the RSM results follow closely the experimental characteristic. The improvement of the agreement with measurements is substantial, compared to the $k-\varepsilon$ results (Fig. 4). Examination of the spanwise distribution of pitchwise-averaged total pressure p_{t_M} at station 4, for various operating points shows that the improvement is mainly due to the accurate prediction between 40% and 80% span (Fig. 4), where the RSM results closely follow the experimental data, improving upon the $k-\varepsilon$ computations. There is also noticeable improvement in predicting the p_{t_M} deficit near the hub (where the non-simulated massflow leakage might account for the remaining discrepancy), for all operating points (Fig. 4). On the other hand the RSM model fails to correct the parasite p_{t_M} peak near the casing, indicating that the relaxation behaviour of the model must be improved. Comparison of computed and measured spanwise distributions of pitchwise-averaged absolute flow angle α_M at station 4 for the different operating points (Fig. 4) shows good agreement between the 2 models and the experiment. The RSM results underestimate α_M by $\sim$1 deg, which is within measurement accuracy [78], whereas the $k-\varepsilon$ results are very close to the experimental data.

In order to understand the mechanism responsible for the improved agreement with measurements, the isentropic Mach-number distributions M_{is} [69] at 70% span (Fig. 5) are examined. At operating point 1 the RSM results predict a flow at the limit between started and unstarted régime [104], whereas the $k-\varepsilon$ computations indicate that the flow is started, with a clearly visible pressure-side shock-wave (Fig. 5). On the suction-side the RSM results predict a shock-wave location $\sim 5\%\chi_x$ further upstream compared to the $k-\varepsilon$ computations (Fig. 5). This point is choked, so that the correspondance between experiment and computations is taken at the same pressure-ratio (and same massflow), corresponding to different shock-structures in the 2 models. For all the other operating points the flow is unstarted [104], with the RSM results predicting the suction-side shock-wave systematically $\sim 5\%\chi_x$ (χ_x=axial chord) upstream of the $k-\varepsilon$ location. Similar conclusions are drawn at other spanwise locations. It is plausible that the main improvement brought by the RSM closure is an improved prediction of the limit between started and unstarted flow, attributed to a better prediction of blockage [78], because of a better prediction of shock-wave/boundary-layer interaction. Another improvement of the RSM closure is a more pronounced p_{t_M} peak very near the hub (Fig. 4), for all operating points, indicating a better prediction of hub secondary flows.

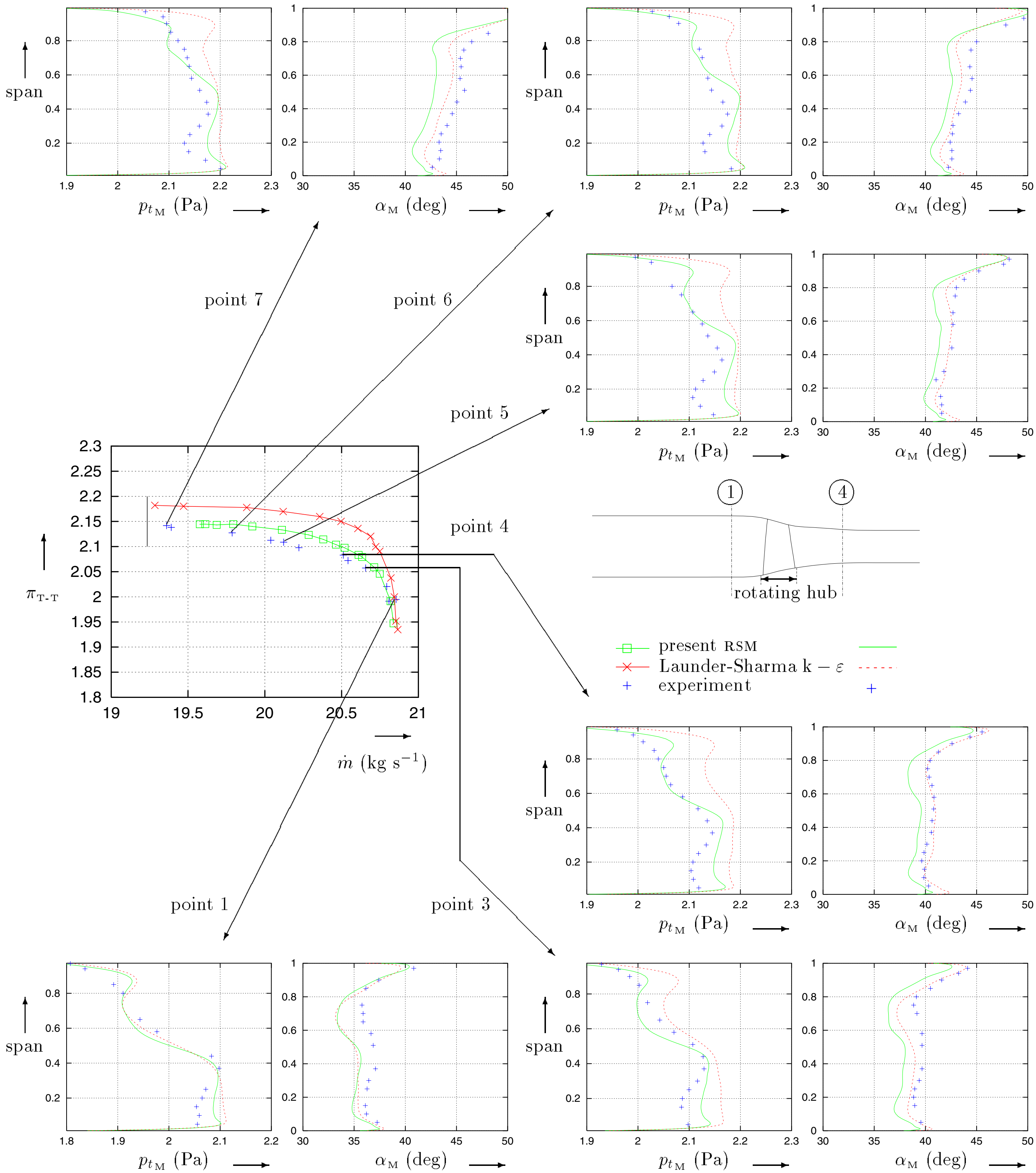

Figure 4: Comparison of measured and computed (using the presen tRSM and the Launder-Sharma k $-\varepsilon$ [58]) radial distributions of pitchwise-averaged flow-angle $\alpha_{x\theta_M}$, and total-pressure p_{t_M}, for various operating points at design-speed, for NASA_37 rotor ($\dot{m}$ =20.85, 20.79, 20.65, 20.51, 20.12, 19.78, 19.36 kg s^{-1}; T_u = 3%; δ_{TC} = 0.356 mm; grid_D).

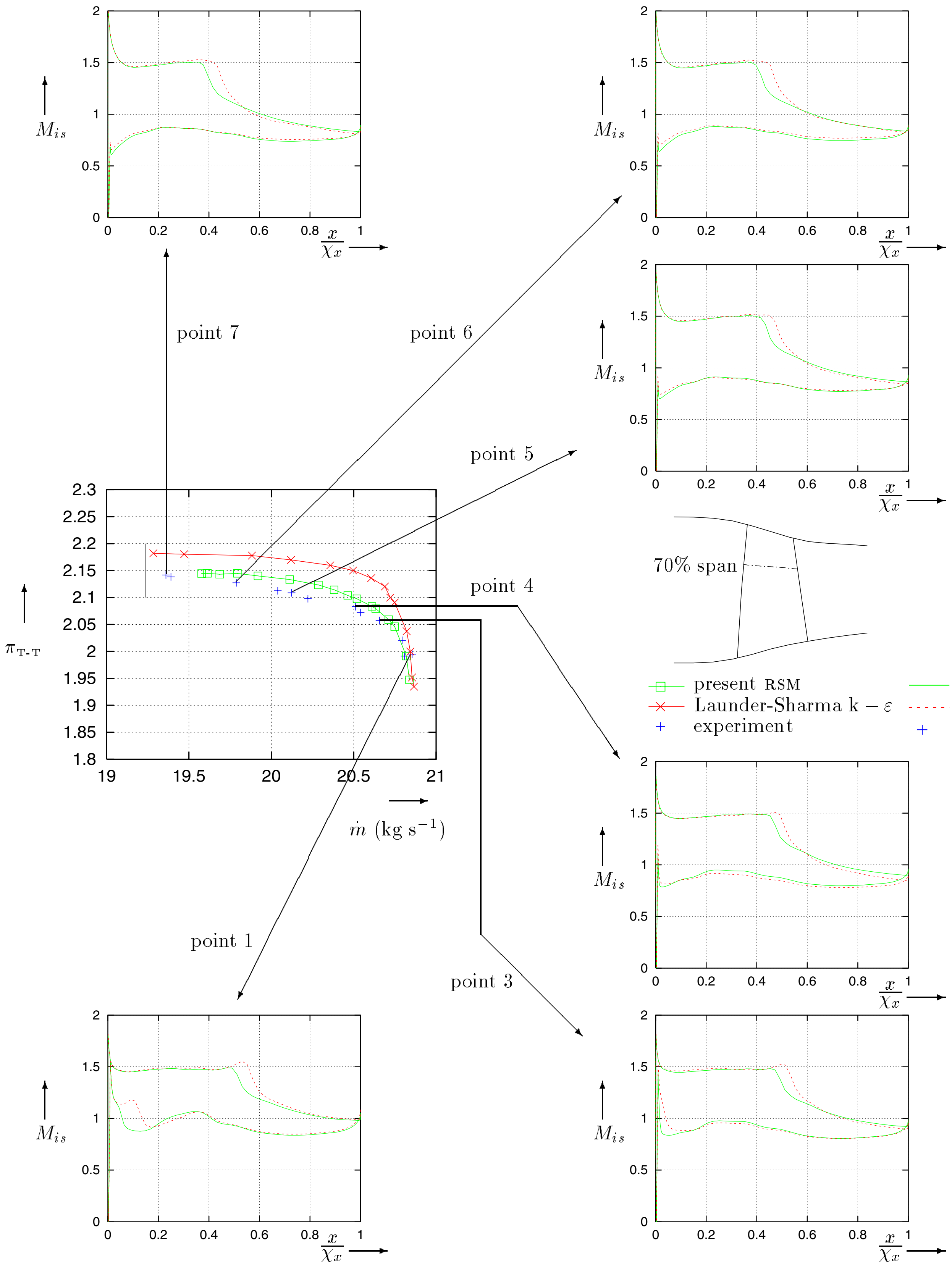

Figure 5: Computed (using the present RSM and the Launder-Sharma k − ε [58]) isentropic-Mach-number distributions at 70% span for various operating points at design-speed, for NASA_37 rotor ($\dot{m}$ =20.85, 20.79, 20.65, 20.51, 20.12, 19.78, 19.36 kg s^{-1}; T_u = 3%; $\delta_{\text{TC}} = 0.356$ mm; grid_D).

Turbine $1\frac{1}{2}$ Stage

Finally computations were run for a $1\frac{1}{2}$stage axial flow turbine, experimentally investigated at the Institut für Strahlantriebe und Turboarbeitsmaschinen of the RWTH [79] [80]. Steady 3-D multistage computations for this configuration (Table 3) have been compared with measurements by Emunds et al. [105], who used a mixing-length turbulence model [23]. Volmar et al. [106] have performed unsteady computations with time-lagged pitchwise periodicity for this configuration, using a $k-\varepsilon$ model [27]. Gallus et al. [107] have performed both steady and unsteady computations, for the stage without the outlet-guide-vane, using a $k-\varepsilon$ model [27].

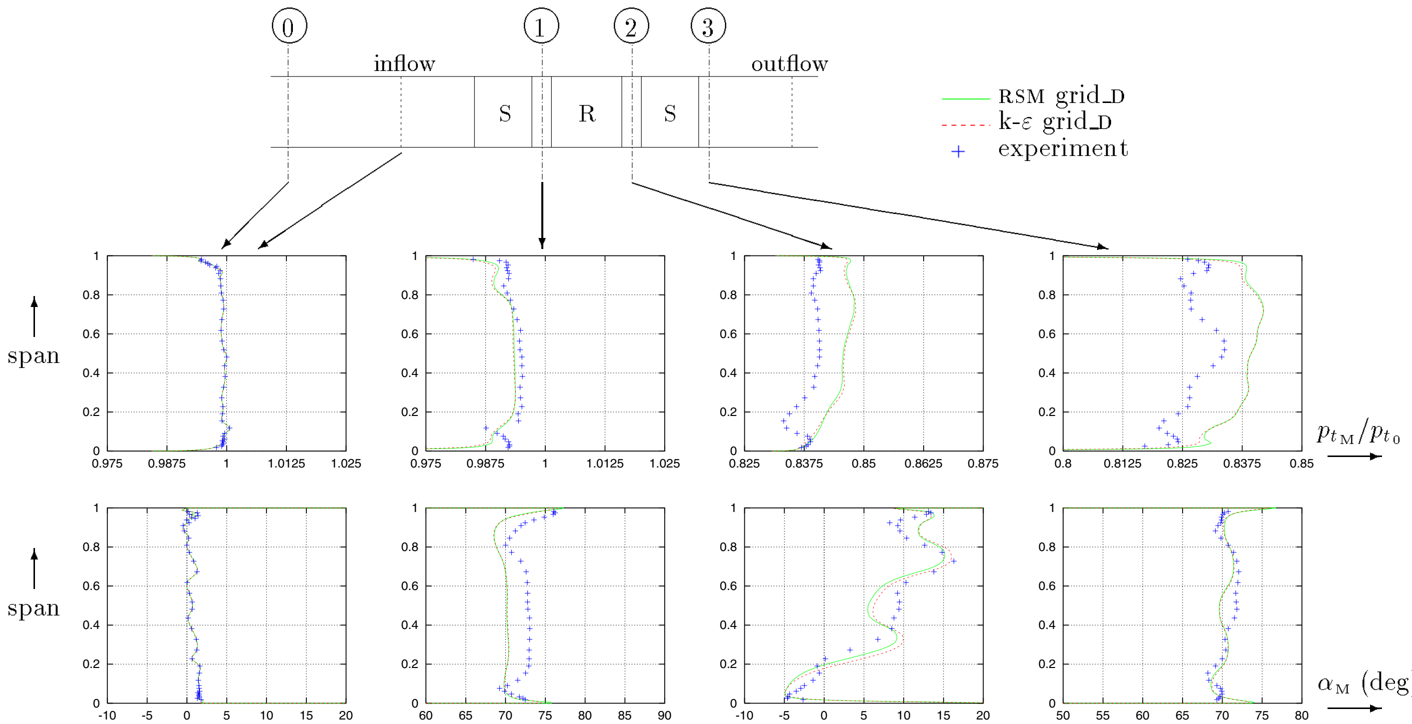

Figure 6: Measured and computed (using the present RSM and the Launder-Sharma $k-\varepsilon$ [58]) radial distributions of pitchwise-averaged total pressure p_{t_M} and flow angle α_M for RWTH_1 turbine $1\frac{1}{2}$stage ($\dot{m} = 8.23$ kg s^{-1}; $T_u = 3\%$; $\delta_{TC} = 0.4$ mm; grid_D).

In the present work we have performed steady-multistage computations using 4 different grids of 1, 2.3, 3, and 4.4×10^6 points (Table 4) with 51, 65, 81, and 121 radial stations, respectively. The multistage method is based on a mixing-plane approach between blade-rows, and is described in detail in Gerolymos and Hanisch [57]. The meridional averages that are conserved across the interface are density, mass-weighted velocities, static pressure, Reynolds-stresses and kinetic-energy-dissipation-rate [57]. The matching between rows is achieved using overlapping grids that allow matching of both values and throughflow-wise gradients of the conserved quantities, ensuring very good continuity at the interfaces [57].

Comparison of measured and computed pitchwise-averaged total pressure p_{t_M} and absolute flow-angle α_M at various axial stations (Fig. 6) indicates that there is close agreement between the RSM and the $k-\varepsilon$ computations on the fine grid_D (4.4×10^6 points). Agreement with measurements is good for the flow-angles α_M, but the computations slightly overestimate the total pressure p_{t_M} at rotor exit (plane 2), and as a consequence at the stage exit plane 3. This overestimation corresponds to a ~1.5% underestimation of turbine expansion ratio.

The form of the radial distribution of p_{t_M} is nonetheless very well predicted (Fig. 6). Volmar et al. [106] note that there are some slight inconsistencies in the experimental data (measurements were taken at different planes for slightly different values of $\dot{m}$, and different values of inlet total pressure p_{t_0}). In our computations the same problems were encountered. As there was some uncertainty concerning massflow, it was preferred to run the computations at a massflow $\dot{m} = 8.23$ kg s^{-1} slightly higher than the average experimental massflow $\dot{m}_{\exp} = 8$ kg s^{-1}, so as to have good agreement

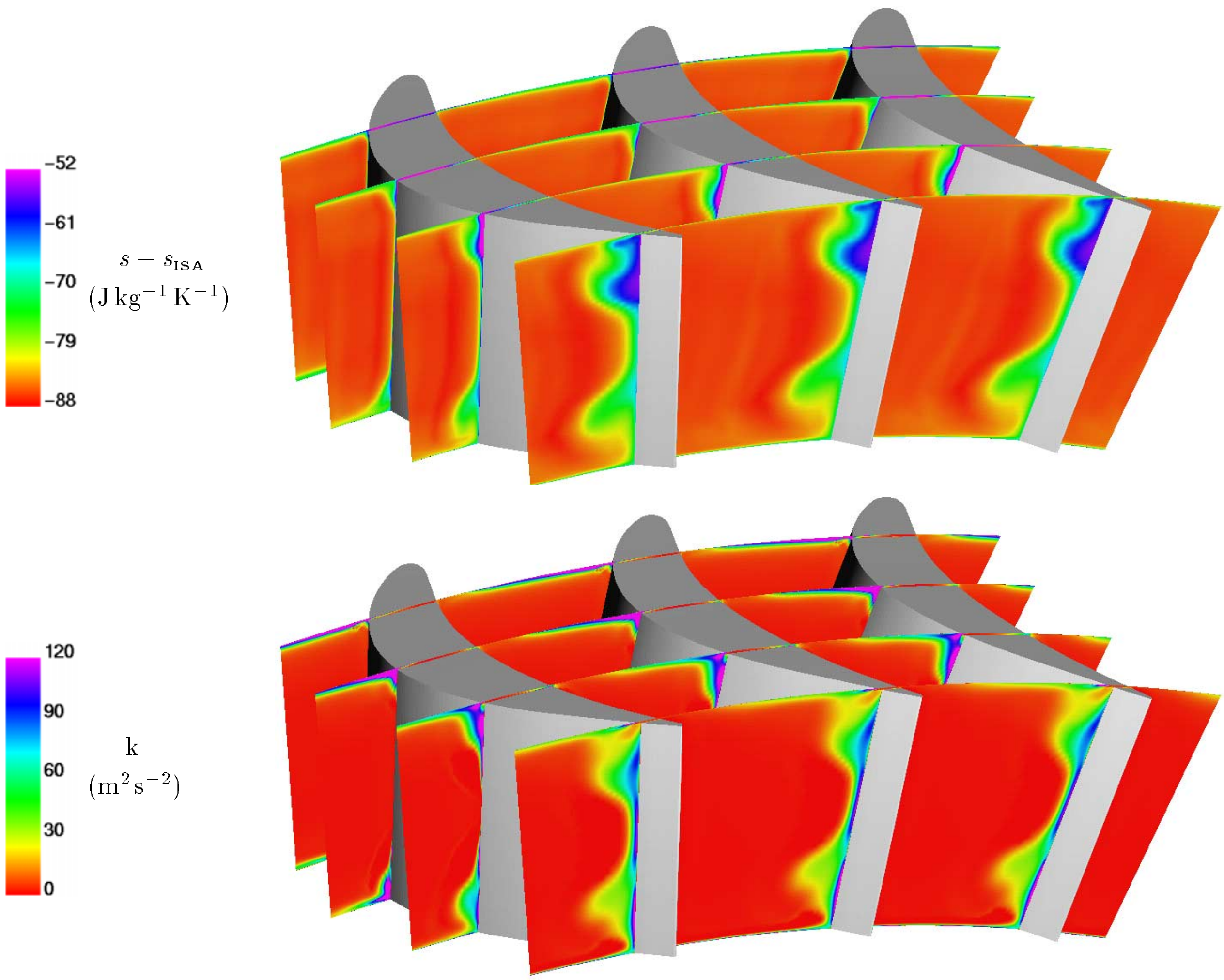

Figure 7: Computed entropy and turbulent kinetic energy plots at various axial planes in the rotor of the RWTH_1 turbine $1\frac{1}{2}$stage ($\dot{m} = 8.23$ kg s^{-1}; $T_u = 3\%$; $\delta_{\mathrm{TC}} = 0.4$ mm; RSM grid_D).

in rotor outflow (plane 2) angle α_{M} (Fig. 6). This resulted in the slight difference in $p_{t_{\mathrm{M}}}$ level. This choice (instead of fitting $p_{t_{\mathrm{M}}}$ with a corresponding discrepancy in α_{M}) was taken because of our interest in the secondary flow phenomena at rotor exit (Fig. 7). Each peak on the rotor-exit α_{M} (Fig. 6) distribution can be identified with a secondary flow-peak in entropy and turbulence-kinetic energy distributions (Fig. 7). The overall agreement with measurements is quite good, for both turbulence models, except at ~20% span, where a slight dip in α_{M}, associated with an important dip in $p_{t_{\mathrm{M}}}$ is not correctly predicted. Emunds et al. [105] argue that this location corresponds to the interaction between the nozzle-hub and the rotor-hub secondary vortices.

The grid influence on results is illustrated by comparing the results obtained using the different grids (Table 4) and the 2 turbulence models for the α_{M} distribution at rotor exit (Fig. 8). Concerning the RSM computations, it is seen that the coarsest grid_A with 51 radial stations fails to predict correctly the structure of the secondary flows. It should be noted that this grid has unacceptably high values of $n_w^+ \cong 5 - 10$ (Table 4). The RSM computations on grid_B with 65 radial stations and $n_w^+ \sim \frac{3}{2}$ (Table 4) does a good job in predicting the structure of the secondary flows everywhere, except near the casing where it fails to correctly describe the tip-leakage vortex, associated with the α_{M}-peak at 96% span (Fig. 8). This is improved in the RSM computations on grid_C which has 81 radial stations, $n_w^+ < 1$, and a finer grid within the tip-clearance-gap (Table 4). This grid predicts the tip-leakage vortex α_{M}-peak at 96% span, but not the ondulation at 90% span, corresponding to the

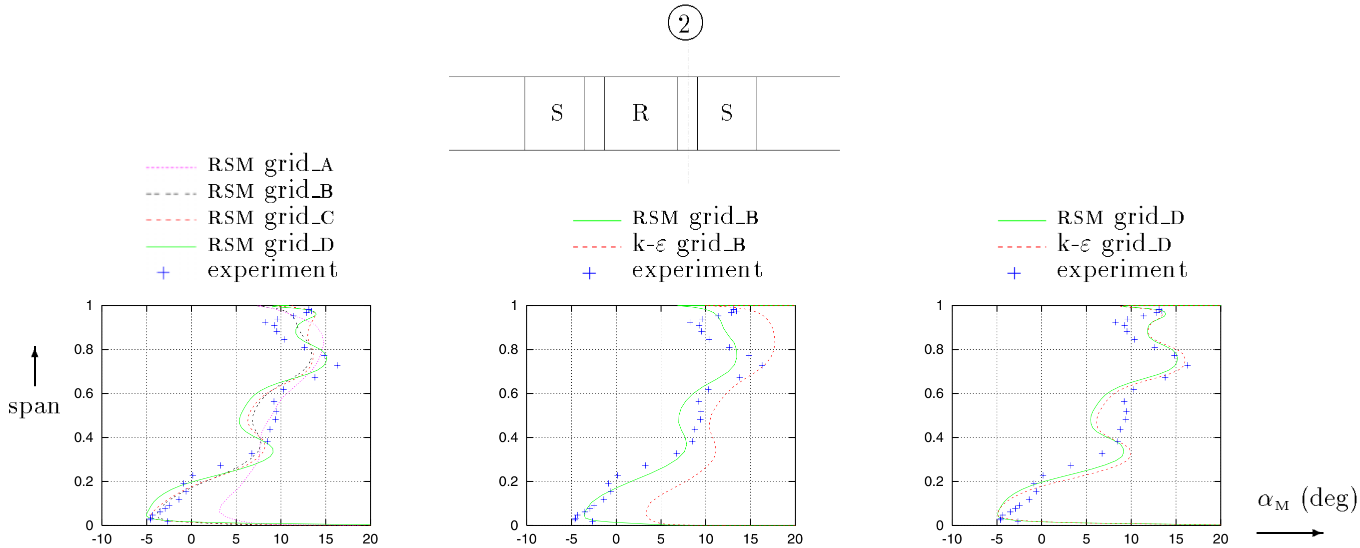

Figure 8: Grid-influence on pitchwise-averaged absolute-flow angle $\alpha_{\rm M}$ at rotor-exit of RWTH_1 $1\frac{1}{2}$stage turbine ($\dot{m} = 8.23$ kg s^{-1}; $T_u = 3\%$; $\delta_{\rm TC} = 0.4$ mm; grid_D).

interaction between tip-clearance and the casing secondary vortex (Fig. 8). Finally the RSM computations on grid_D with 121 radial stations predict correctly the secondary flows. Examination of the $\mathrm{k}-\varepsilon$ computations on grid_B and grid_D reveals the interesting feature that although both models give similar results on the fine grid_D, the RSM computations are substantially better on the coarse grid_B, compared to the $\mathrm{k}-\varepsilon$ computations on the same grid (Fig. 8).

Conclusions and Perspectives in Turbulence Modelling

In the present work a new near-wall low-turbulence-Reynolds-number Reynolds-stress model (RSM), that has been designed to be completely independent of wall-topology (distance-from-the-wall and normal-to-the-wall orientation), has been evaluated by comparison with experimental measurements, and with results using the Launder-Sharma $\mathrm{k}-\varepsilon$ model, for 3 turbomachinery configurations. To the authors knowledge this is the first time that a full near-wall second-moment closure is applied to complex 3-D turbomachinery configurations.

For the NTUA_1 subsonic annular cascade, the RSM closure corrects the deficiency of the $\mathrm{k}-\varepsilon$ model, by predicitng the large suction-side hub-corner-stall observed experimentally. This results in a substantially improved prediction of cascade-exit flow-angle distribution, resulting from a better prediction of the complex 3-D separated flow structure.

For the NASA_37 transonic compressor rotor, the RSM closure improves the massflow *vs.* pressure-ratio operating-map prediction, by improving the prediction of the radial distribution of total-pressure, through a better prediction of rotor-shock-wave structure (and of shock-wave/boundary-layer interaction). In particular, the rotor spill-point (where the flow at the tip becomes unstarted) is correctly predicted.

For the RWTH_1 $1\frac{1}{2}$ stage axial flow turbine, both models give good prediction of the flow, with the RSM model being less-grid-sensitive than the $\mathrm{k}-\varepsilon$ model, an important advantage for industrial applications on relatively coarse grids. In this case the $\mathrm{k}-\varepsilon$ results on the fine grid are very satisfactory, because there is no substantial flow separation.

Globally the present RSM closure yields invariably better results than the $\mathrm{k}-\varepsilon$ closure, especially when flow separation dominates the flowfield. For flows with little separation the improvement is marginal, but for all the configurations studied by the authors results are invariably better with the RSM closure. Experience with the model shows that it is as robust as the $\mathrm{k}-\varepsilon$ model, and computing time-requirements are only 30% higher per iteration. When the RSM closure captures complex separated flow structures, convergence may be slower so that a factor 1.5 in overall computing-time requirements is estimated.

The basic drawback of the model, as established from comparisons with experimental data for basic shock-wave/boundary-layer interaction flows, is a too slow relaxation after the interaction, and a delayed reattachment. As a consequence blockade is slightly overpredicted. Furthermore the model does not improve upon the $\mathrm{k}-\varepsilon$ results in the prediction of the tip-clearance vortex mixing with the main flow, but this is again a problem of too slow relaxation (mainly observed in the $p_{t_{\rm M}}$-peak near the casing for the NASA_37 rotor case). In summary the new model correctly predicts separation, but should be improved in the prediction of reattachment. These are 2 different processes. The separation has been controlled in the model by an improved quasi-linear model of the rapid pressure-strain term. The control of reattachement (independently of separation) is currently under investigation (improved ε equation, or 2-scale model).

Despite the aforementionned drawbacks, the new RSM offers more confidence in CFD results than 2-equation closures, and also more possibilities for improvements, since it offers a better description of turbulence structure. It is believed that further validation work, and further developments in such advanced turbulence closures (as opposed to oversimplified 1-equation closures) will improve the state-of-the-art of turbomachinery CFD.

Acknowledgments

The computations presented were run at the Institut pour le Développement des Ressources en Informatique Scientifique (IDRIS), where computer ressources were made available by the Comité Scientifique. The research scholarships of V.C.S. and J.N. were funded through the APPACET project (BRITE project of the European Community). Authors are listed alphabetically.

References

[1] Adamczyk, J.J., "Model Equation for Simulating Flows in Multistage Turbomachinery," ASME Paper 85–GT–226, 1985.

[2] Dawes, W.N., "Toward Improved Throughflow Capability: The Use of 3-D Viscous Flow Solvers in a Multistage Environment," *J. Turbom.*, Vol. 114, 1992, pp. 8–17.

[3] Denton, J.D., "The Calculation of 3-D Viscous Flow through Multistage Turbomachines," *J. Turbom.*, Vol. 114, 1992, pp. 18–26.

[4] Erdos, J.I., Alzner, E., and McNally W., "Numerical Solution of Periodic Transonic Flow through a Fan Stage," *AIAA J.*, Vol. 15, 1977, pp. 1559–1568.

[5] Giles, M.B., "Stator/Rotor Interaction in a Transonic Turbine," *J. Prop. Power*, Vol. 6, 1990, pp. 621–627.

[6] He, L., "Method of Simulating Unsteady Turbomachinery Flows with Multiple Perturbations," *AIAA J.*, Vol. 30, 1992, pp. 2730–2735.

[7] Rieß, W., and Evers, B., "Die Strömung in mehrstufigen Turbinen mit langen Schaufeln bei Schwachlast- und Leerlaufbetrieb," *VGB Kraftwerkstechnik*, Vol. 65, 1985, pp. 1020–1026.

[8] Leylek, J.H., and Wisler, D.C., "Mixing in Axial-Flow Compressors: Conclusions Drawn from 3-D Navier-Stokes Analyses and Experiments," *J. Turbom.*, Vol. 113, 1991, pp. 139–160.

[9] Suder, K.L., Chima, R.V., Strazisar, A.J., and Roberts, W.B., "The Effect of Adding Roughness and Thickness to a Transonic Axial Compressor Rotor," *J. Turbom.*, Vol. 117, 1995, pp. 491–505.

[10] Denton, J.D., "Loss Mechanisms in Turbomachines," *J. Turbom.*, Vol. 115, 1993, pp. 621–656.

[11] Adamczyk, J.J., "Aerodynamic Analysis of Multistage Turbomachinery Flows in Support of Aerodynamic Design," *J. Turbom.*, Vol. 122, 2000, pp. 189–217.

[12] Silkowski, P.D., and Hall, K.C., "A Coupled Mode Analysis of Unsteady Multistage Flows in Turbomachinery," *J. Turbom.*, Vol. 120, 1998, pp. 410–421.

[13] Shabbir, A., Celestina, M.L., Adamczyk, J.J., and Strazisar, A.J., "The Effect of Hub Leakage on 2 High Speed Axial Flow Compressor Rotors," ASME Paper 97–GT–346, 1997.

[14] Wellborn, S.R., and Okiishi, T.H., "The Influence of Shrouded Cavity Flows on Multistage Compressor Performance," *J. Turbom.*, Vol. 121, 1999, pp. 486–498.

[15] Wellborn, S.R., Tolchinsky, I., and Okiishi, T.H., "Modeling Shrouded Stator Cavity Flows in Axial-Flow Compressors," *J. Turbom.*, Vol. 121, 1999, pp. 486–498.

[16] Lakshminarayana, B., "Turbulence Modeling for Complex Shear Flows," *AIAA J.*, Vol. 24, 1986, pp. 1900–1917.

[17] Mayle, R.E., "The Role of Laminar-Turbulent Transition in Gas Turbine Engines," *J. Turbom.*, Vol. 113, 1991, pp. 509–537.

[18] Bradshaw, P., "Turbulence Modeling with Application to Turbomachinery," *Prog. Aerospace Sci.*, Vol. 32, 1996, pp. 575–624.

[19] Hah, C., "A Numerical Modeling of Endwall and Tip-Clearance Flow of an Isolated Compressor Rotor," *J. Eng. Gas Turb. Power*, Vol. 108, 1986, pp. 15–21.

[20] Hah, C., "Calculation of 3-D Viscous Flows in Turbomachinery with an Implicit Relaxation Method," *J. Prop. Power*, Vol. 3, 1987, pp. 415–422.

[21] Dawes, W.N., "A Numerical Analysis of the 3-D Viscous Flow in a Transonic Compressor Rotor and Comparison with Experiment," *J. Turbom.*, Vol. 109, 1987, pp. 83–90.

[22] Goyal, R.K., and Dawes, W.N., "A Comparison of the Measured and Predicted Flow Field in a Modern Fan-Bypass Configuration," *J. Turbom.*, Vol. 115, 1993, pp. 273–282.

[23] Baldwin, B., and Lomax H., "Thin-Layer Approximation and Separated Algebraic Model for Separated Turbulent Flows," AIAA Paper 78–257, 1978.

[24] Hah, C., Bryans, A.C., Moussa, Z., and Tomsho, M.E., "Application of Viscous Flow Computations for the Aerodynamic Performance of a Backswept Impeller at Various Operating Conditions," *J. Turbom.*, Vol. 110, 1988, pp. 303–311.

[25] Copenhaver, W.W., Hah, C., and Puterbaugh, S.L., "3-D Flow Phenomena in a Transonic, High-Throughflow, Axial-Flow Compressor Stage," *J. Turbom.*, Vol. 115, 1993, pp. 240–248.

[26] Hah, C., and Loellbach, J., "Development of Hub Corner Stall and Its Influence on the Performance of Axial Compressor Blade Rows," *J. Turbom.*, Vol. 121, 1999, pp. 67–77.

[27] Chien, K.Y., "Predictions of Channel and Boundary-Layer Flows with a Low-Reynolds Number Turbulence Model," *AIAA J.*, Vol. 20, No. 1, 1982, pp. 33–38.

[28] Adamczyk, J.J., Celestina, M.L., Beach, T.A., and Barnett, M., "Simulation of 3-D Viscous Flow within a Multistage Turbine," *J. Turbom.*, Vol. 112, 1990, pp. 370–376.

[29] Mulac, R.A., and Adamczyk, J.J., "The Numerical Simulation of a High-Speed Axial Flow Compressor," *J. Turbom.*, Vol. 114, 1992, pp. 517–527.

[30] Adamczyk, J.J., Celestina, M.L., and Greitzer, E.M., "The Role of Tip Clearance in High-Speed Fan Stall," *J. Turbom.*, Vol. 115, 1993, pp. 28–39.

[31] Chima, R.V., and Yokota, J.W., "Numerical Analysis of 3-D Viscous Internal Flows," *AIAA J.*, Vol. 28, 1990, pp. 798–806.

[32] Chima, R.V., "Calculation of Tip Clearance Effects in a Transonic Compressor Rotor," *J. Turbom.*, Vol. 120, 1998, pp. 131–140.

[33] Kunz, R.F., and Lakshminarayana, B., "3-D Navier-Stokes Computation of Turbomachinery Flows using an Explicit Numerical Procedure and a Coupled $k - \varepsilon$ Turbulence Model," *J. Turbom.*, Vol. 114, 1992, pp. 627–642.

[34] Kunz, R.F., Lakshminarayana, B., and Basson, A.H., "Investigation of Tip-Clearance Phenomena in an Axial Compressor Cascade using Euler and Navier-Stokes Procedures," *J. Turbom.*, Vol. 115, 1993, pp. 453–467.

[35] Koiro, M., and Lakshminarayana, B., "Simulation and Validation of Mach-Number Effects on Secondary Flow in a Transonic Turbine Cascade using a Multigrid $k - \varepsilon$ Solver," *J. Turbom.*, Vol. 120, 1998, pp. 285–297.

[36] Dawes, W.N., "The Simulation of 3-D Viscous Flow in Turbomachinery Geometries using a Solution-Adaptive Unstructured Mesh Methodology," *J. Turbom.*, Vol. 114, 1992, pp. 528–537.

[37] Dawes, W.N., "The Extension of a Solutions-Adaptive 3-D Navier-Stokes Solver toward Geometries of Arbitrary Complexity," *J. Turbom.*, Vol. 115, 1993, pp. 283–295.

[38] Lam, C.K.G., and Bremhorst, K.A., "Modified Form of the $k-\varepsilon$ Model for Predicting Wall Turbulence," *J. Fluids Eng.*, Vol. 103, 1981, pp. 456–460.

[39] Rizzi, A., Eliasson, P., Lindblad, I., Hirsch, C., Lacor, C., and Haeuser, J., "The Engineering of Multiblock/Multigrid Software for Navier-Stokes Flows on Structured Meshes," *Comp. Fluids*, Vol. 22, 1993, pp. 341–367.

[40] Kang, S., and Hirsch, C., "Numerical Simulation of 3-D Viscous Flow in a Linear Compressor Cascade with Tip-Clearance," *J. Turbom.*, Vol. 118, 1996, pp. 492–505.

[41] Arnone, A., Liou, M.S., and Povinelli, L.A., "Multigrid Calculation of 3-D Viscous Cascade Flows," *J. Prop. Power*, Vol. 9, 1993, pp. 605–614.

[42] Ameri, A.A., and Arnone, A., "Transition Modeling Effects on Turbine Rotor Blade Heat Transfer Predictions," *J. Turbom.*, Vol. 118, 1996, pp. 307–313.

[43] Arnone, A., "Viscous Analysis of 3-D Rotor Flow using a Multigrid Method," *ASME J. Turbom.*, Vol. 116, 1994, pp. 435–445.

[44] Turner, M.G., and Jennions, I.K., "An Investigation of Turbulence Modeling in Transonic Fans Including a Novel Implementation of an Implicit $k-\varepsilon$ Turbulence Model," *J. Turbom.*, Vol. 115, 1993, pp. 249–260.

[45] Jennions, I.K., and Turner, M.G., "3-D Navier-Stokes Computations of Transonic Fan Flow using an Explicit Flow Solver and an Implicit $k-\varepsilon$ Turbulence Model," *J. Turbom.*, Vol. 115, 1993, pp. 261–272.

[46] Launder, B.E., and Spalding, D.B., "The Numerical Computation of Turbulent Flows," *Comp. Meth. Appl. Mech. Eng.*, Vol. 3, 1974, pp. 269–289.

[47] Langowsky, C., and Vogel, D.T., "Influence of Film-Cooling on the Secondary Flow in a Turbine Nozzle," *AIAA J.*, Vol. 35, 1997, pp. 111–118.

[48] Hildebrandt, T., and Fottner, L., "A Numerical Study of the Influence of Grid Refinement and Turbulence modeling on the Flow Field Inside a Highly Loaded Turbine Cascade," *J. Turbom.*, Vol. 121, 1999, pp. 709–716.

[49] Wilcox, D.C., "Simulation of Transition with a 2-Equation Turbulence Model," *AIAA J.*, Vol. 32, 1994, pp. 247–255.

[50] Ameri, A.A., Steinthorsson, E., and Rigby, D.L., "Effect of Squealer Tip on Rotor Heat Tranfer and Efficiency," *J. Turbom.*, Vol. 120, 1998, pp. 753–759.

[51] Ameri, A.A., Steinthorsson, E., and Rigby, D.L., "Effects of Tip-Clearance and Casing Recess on Heat Transfer and Stage Efficiency in Axial Turbines," *J. Turbom.*, Vol. 121, 1999, pp. 683–693.

[52] Furukawa, M., Inoue, M., Saiki, K., Yamada, K., "The Role of Tip Leakage Vortex Breakdown in Compressor Rotor Aerodynamics," *J. Turbom.*, Vol. 121, 1999, pp. 469–480.

[53] Rhie, C.M., Gleixner, A.J., Spear, D.A., Fischberg, C.J., Zacharias, R.M., "Development and Application of a Multistage Navier-Stokes Solver: Part I — Multistage Modeling using Bodyforces and Deterministic Stresses," *J. Turbom.*, Vol. 120, 1998, pp. 205–214.

[54] LeJambre, C.R., Zacharias, R.M., Biederman, B.P., Gleixner, A.J., Yetka, C.J., "Development and Application of a Multistage Navier-Stokes Solver: Part II — Application to a High-Pressure Compressor Design," *J. Turbom.*, Vol. 120, 1998, pp. 215–223.

[55] Gerolymos, G.A., G. Tsanga, and Vallet, I., "Near-Wall $k-\varepsilon$ Computation of Transonic Turbomachinery Flows with Tip-Clearance," *AIAA J.*, Vol. 36, 1998, pp. 1769–1777.

[56] Gerolymos, G.A., and Vallet, I., "Tip-Clearance and Secondary Flows in a Transonic Compressor Rotor," *J. Turbom.*, Vol. 121, 1999, pp. 751–762.

[57] Gerolymos, G.A., and Hanisch, C., "Multistage 3-D Navier-Stokes Computation of Off-Design Operation of a 4-Stage Turbine," *IMechE J. Power Energy*, Vol. 213, 1999, pp. 243–261.

[58] Launder, B.E., and Sharma, B.I., "Application of the Energy Dissipation Model of Turbulence to the Calculation of Flows near a Spinning Disk," *Lett. Heat Mass Transf.*, Vol. 1, 1974, pp. 131–138.

[59] Arima, T., Sonoda, T., Shirotori, M., Tamura, A., and Kikuchi, K., "A Numerical Investigation of Transonic Axial Compressor Rotor Flow using a Low-Reynolds-Number $k-\varepsilon$ Turbulence Model," *J. Turbom.*, Vol. 121, 1999, pp. 44–58.

[60] Hoeger, M., Fritsch, G., and Bauer, D., "Numerical Simulation of the Shock/Tip-Leakage-Vortex Interaction in a HPC Front Stage," *J. Turbom.*, Vol. 121, 1999, pp. 456–468.

[61] Fritsch, G., Hoeger, M., Blaha, C., and Bauer, D., "Viscous 3-D Simulation of Transonic Compressor Stage on Parallel Hardware," *J. Prop. Power*, Vol. 16, 2000, pp. 388–396.

[62] Sleiman, M., Tam, A., Robichaud, M.P., Peeters, M.F., and Habashi, W.G., "Multistage Simulation by an Adaptive Finite Element Approach using Strucutred Grids," *J. Fluids Eng.*, Vol. 121, 1999, pp. 450–459.

[63] Sayma, A.I., Vahdati, M., Sbardella, L., and Imregun, M., "Modeling of 3-D Viscous Compressible Turbomachinery Flows using Unstructured Hybrid Grids," *AIAA J.*, Vol. 38, 2000, pp. 945–954.

[64] Baldwin, B.S., and Barth, T.J., "1-Equation Turbulence Transport Model for High-Reynolds-Number Wall-Bounded Flows," AIAA Paper 91–0610, 1991.

[65] Launder, B.E., "2-Moment Closure and its Use in Modelling Turbulent Industrial Flows," *Int. J. Num. Meth. Fluids*, Vol. 9, 1989, pp. 963–985.

[66] Hanjalić, K., "Advanced Turbulence Closure Models: A View of Current Status and Future Prospects," *Int. J. Heat Fluid Flow*, Vol. 15, 1994, pp. 178–203.

[67] Leschziner, M.A., "Computation of Aerodynamic Flows with Turbulence-Transport Models Based on 2-Moment Closure," *Comp. Fluids*, Vol. 24, 1995, pp. 377–392.

[68] Gerolymos, G.A., and Vallet, I., "Wall-Normal-Free Near-Wall Reynolds-Stress Closure for 3-D Compressible Separated Flows," *AIAA J.*, submitted december 24 1999.

[69] Gerolymos, G.A., and Vallet, I., "Wall-Normal-Free Reynolds-Stress Prediction of 3-D Turbomachinery Flows," *AIAA J.*, submitted september 9 2000.

[70] Noussis, I., "Validation d'une Fermeture RSMsur des Profils d'Aile," DEA, Université Pierre-et-Marie-Curie, Paris, 2000.

[71] Filaire, F., "Evaluation des Possibilités Prédictives es Modélisations de l'Interaction Choc/Couche-Limite," DEA, Université Pierre-et-Marie-Curie, Paris, 2000.

[72] Doukelis, A., Mathioudakis, K., Papailiou, K., "The Effect of Tip Clearance Gap Size and Wall Rotation on the Performance of a High-Speed Annular Compressor Cascade," *ASME Paper*, 98-GT-38, 1998.

[73] Doukelis, A., Mathioudakis, K., Papailiou, K., "Investigation of the 3-D Flow Structure in a High-Speed Annular Compressor Cascade for Tip Clearance Effects," *ASME Paper*, 98-GT-39, 1998.

[74] Doukelis, A., Mathioudakis, K., Papailiou, K., "Detailed Flow and Overall Performance Measurements for Different Clearance Configurations in the NTUA Annular Cascade Facility," Chapter 3, Final Report, APPACET Project, EEC Conract BRPR-CT97-0610, 2000.

[75] Strazisar, A.J., "Data Report and Data Diskette for NASA Transonic Compressor Rotor 37," NASA Lewis Research Center, 1994.

[76] Davis, R.L., Delaney, R.A., Denton, J.D., Giles, M.B.,, Strazisar, A.J., and Wisler, D.C., 1993, "CFD Code Assessment in Turbomachinery — Author's Information Package," ASME Turbomachinery Committee.

[77] Denton, J.D., "Lessons Learned from Rotor 37," 3. International Symposium on Experimental and Computational Aerothermodynamics of Internal Flows (ISAIF), Beijing, China, September 1–6, 1996.

[78] Suder, K.L., "Blockage Develpment in a Transonic Axial Compressor Rotor," *J. Turbom.*, Vol. 120, 1998, pp. 465–476.

[79] Walraevens, R.E., and Gallus, H.E., "Stator-Rotor-Stator Interaction in an Axial Flow Turbine and its Influence on Loss Mechanisms," *AGARD Conf. Proc.*, Vol. 571, 1996, pp. 39·1–39·14.

[80] Walraevens, R.E., Gallus, H.E., Jung, A.R., Mayer, J.F., and Stetter, H., "Experimental and Computational Study of the Unsteady Flow in a $1\frac{1}{2}$Stage Axial Turbine with Emphasis on the Secondary Flow in the Second Stator," ASME Paper 98–GT–254, 1998.

[81] Aris, R., *Vectors, Tensors, and the Basic Equations of Fluid Mechanics*, 1962, Dover, New York (ISBN 0–486–66110–5).

[82] Hanjalić, K., and Launder, B.E., "A Reynolds Stress Model of Turbulence and its Application to Thin Shear Flows," *J. Fluid Mech.*, Vol. 52, 1972, pp. 609–638.

[83] Launder, B.E., and Shima, N., "2-Moment Closure for the Near-Wall Sublayer: Development and Application," *AIAA J.*, Vol. 27, 1989, pp. 1319–1325.

[84] Launder, B.E., Tselepidakis, D.P., and Younis, B.A., "A Second-Moment Closure Study of Rotating Channel Flow," *J. Fluid Mech.*, Vol. 183, 1987, pp. 63–75.

[85] Shima, N., "Prediction of Turbulent Boundary-Layer Flows with a 2-Moment Closure: Part I — Effects of Periodic Pressure Gradient, Wall Transpiration, and Free-Stream Turbulence," *ASME J. Fluids Eng.*, Vol. 115, 1993, pp. 56–63.

[86] Shima, N., "Prediction of Turbulent Boundary-Layer Flows with a 2-Moment Closure: Part II — Effects of Streamline Curvature and Spanwise Rotation," *ASME J. Fluids Eng.*, Vol. 115, 1993, pp. 64–69.

[87] Gibson, M.M., and Launder, B.E., "Ground Effects on Pressure Fluctuations in the Atmospheric Boundary Layer," *J. Fluid Mech.*, Vol. 86, 1978, pp. 491–511.

[88] Lumley, J.L., "Computational Modeling of Turbulent Flows," *Adv. Appl. Mech.*, Vol. 18, 1978, pp. 123–176.

[89] Launder, B.E., and Li, S.P., "Elimination of Wall-Topography Parameters from 2-Moment Closure," *Phys. Fluids*, Vol. 6, 1994, pp. 999–1006.

[90] Gerolymos, G.A., and Vallet, I., "Implicit Computation of the 3-D Compressible Navier-Stokes Equations using $k - \varepsilon$ Turbulence Closure," *AIAA J.*, Vol. 34, 1996, pp. 1320–1321.

[91] Gerolymos, G.A., and Vallet, I., "Near-Wall Reynolds-Stress 3-D Transonic Flows Computation," *AIAA J.*, Vol. 35, 1997, pp. 228–236.

[92] Gerolymos, G.A., and Tsanga, G., "Biharmonic 3-D Grid Generation for Axial Turbomachinery with Tip-Clearance," *J. Prop. Power*, Vol. 15, 1999, pp. 476–479.

[93] Jones, W.P., and Launder, B.E., "The Prediction of Laminarization with a 2-Equation Model of Turbulence," *Int. J. Heat Mass Transf.*, Vol. 15, 1972, pp. 301–314.

[94] Van Driest, E.R., "Turbulent Boundary-Layer in Compressible Fluids," *J. Aero. Sci.*, Vol. 18, 1951, pp. 145–160,216.

[95] Spalding, D.B., "A Single Formula for the Law-of-the-Wall," *ASME J. Appl. Mech.*, Vol. 28, 1961, pp. 455–458.

[96] Coles, D., "The Law of the Wake in the Turbulent Boundary Layer," *J. Fluid Mech.*, Vol. 1, 1956, pp 191–226.

[97] Clauser, F.H., "The Turbulent Boundary-Layer," *Adv. Appl. Mech.*, Vol. 4, 1956, pp. 1–51.

[98] Harris, V.G., Graham, J.A.M, Corrsin, S., "Further experiments in nearly homogeneous turbulent shear flows," *J. Fluid Mech.*, Vol. 81, 1977, pp 657–687.

[99] Gerolymos, G.A., "Implicit Multiple-Grid Solution of the Compressible Navier-Stokes Equations using k $-\ \varepsilon$ Turbulence Closure," *AIAA J.*, Vol. 28, 1990, pp. 1707–1717.

[100] Vallet, I., "Aérodynamique Numérique 3-D Instationnaire avec Fermeture Bas-Reynolds au Second Ordre," Doctorat, Université Pierre-et-Marie-Curie, Paris, December 1995.

[101] Tsanga, G., "Aérodynamique Numérique 3-D des Turbomachines Axiales Multiétages avec Fermeture k $-\ \varepsilon$ Bas-Reynolds," Doctorat, Université Pierre-et-Marie-Curie, Paris, January 1997.

[102] Shabbir, A., Zhu, J., and Celestina, M., "Assessment of 3 Turbulence Models in a Compressor Rotor," ASME Paper 96–GT–198, 1996.

[103] Gregory-Smith, D.G., "Synthesis of Calculations Performed on the NASA Rotor 37," Chapter 5, Final Report, APPACET Project, EEC Conract BRPR-CT97-0610, 2000.

[104] Lichtfuss, H.J., and Starken, H., "Supersonic Cascade Flow," *Progress in Aerospace Sciences*, Vol. 15, 1974, pp. 37–149.

[105] Emunds, R., Jennions, I.K., Bohn, D., and Gier, J., "The Computation of Adjacent Blade-Row Effects in a $1\frac{1}{2}$-Stage Axial Flow Turbine," *J. Turbom.*, Vol. 121, 1999, pp. 1–10.

[106] Volmar, T.W., Brouillet, B., Gallus, H.E., Benetschik, H., "Time-Accurate 3-D Navier-Stokes Analysis of $1\frac{1}{2}$-Stage Axial-Flow Turbine," *J. Prop. Power*, Vol. 16, 2000, pp. 327–335.

[107] Gallus, H.E., Zeschky, J., and Hah, C., "Endwall and Unsteady Flow Phenomena in an Axial Turbine Stage," *J. Turbom.*, Vol. 117, 1995, pp. 562–570.